6-2020

Tension-tension Fatigue Behavior of Nextel™ 720/Alumina-mullite Ceramic Composite at 1200°C in Air and in Steam

Sarah A. Witzgall

TENSION-TENSION FATIGUE BEHAVIOR OF NEXTEL™720/ALUMINA-MULLITE CERAMIC COMPOSITE AT 1200°C IN AIR AND IN STEAM

THESIS

Sarah A. Witzgall, 1st Lt, USAF

AFIT-ENY-MS-20-J-078

DEPARTMENT OF THE AIR FORCE
AIR UNIVERSITY

AIR FORCE INSTITUTE OF TECHNOLOGY

Wright-Patterson Air Force Base, Ohio

AFIT-ENY-MS-20-J-078

TENSION-TENSION FATIGUE BEHAVIOR OF NEXTEL™720/ALUMINA-MULLITE CERAMIC COMPOSITE AT 1200°C IN AIR AND IN STEAM

THESIS

Presented to the Faculty

Department of Aeronautics and Astronautics

Graduate School of Engineering and Management

Air Force Institute of Technology

Air University

Air Education and Training Command

In Partial Fulfillment of the Requirements for the

Degree of Master of Science in Aeronautical Engineering

Sarah A. Witzgall, BS

1st Lt, USAF

June 2020

AFIT-ENY-MS-20-J-078

TENSION-TENSION FATIGUE BEHAVIOR OF NEXTEL™720/ALUMINA-MULLITE CERAMIC COMPOSITE AT 1200°C IN AIR AND IN STEAM

Sarah A. Witzgall, BS

1st Lt, USAF

Committee Membership:

Dr. Marina B. Ruggles-Wrenn, PhD
Chair

Dr. Thomas G. Eason III, PhD
Member

Dr. Eric L. Jones, PhD
Member

AFIT-ENY-MS-20-J-078

Abstract

Uniaxial tension-tension fatigue performance of an oxide-oxide continuous fiber ceramic composite was studied at 1200°C in laboratory air and in steam. The composite is reinforced with laminated, 0/90 mullite/alumina (NEXTEL™720) fibers woven in an eight-harness satin weave and has a porous alumina/mullite matrix. There is no interphase between the fiber and matrix. The composite relies on the porous matrix for crack deflection and flaw tolerance. Tension-tension fatigue was examined for maximum stresses of 45 – 136 MPa in air and in steam. To assess the effects of the steam environment on fatigue performance, experimental results obtained in air are compared to those obtained in steam. Fatigue run-out, defined as survival of 100,000 cycles (27.7 h at a frequency of 1.0 Hz), was achieved at 45 MPa in air and at 120 MPa in steam. The presence of steam had no apparent detrimental effect on fatigue performance. Lower than expected fatigue performance in air is attributed to pre-existing processing defects in the test material (as-processed test panel, and consequently, test specimens appeared bent). The retained properties of all specimens that achieved fatigue run-out were characterized. Composite microstructure, as well as damage and failure mechanisms, were examined.

Acknowledgments

First, I would like to express my deepest gratitude to my faculty advisor, Dr. Marina B. Ruggles-Wrenn, for her guidance, expertise, passion for materials science and engineering, and her continuous support over the past two years. I sincerely could not have asked for a better advisor for my thesis. I would also like to extend my gratitude to the AFIT lab technicians, Mr. Mike Ranft and Mr. Jamie Smith, who spent countless hours with me in the MTS laboratory, for their patience and expertise. Finally, I would like to thank my entire family, especially my mother, for being a phone call away and supporting me through all my endeavors.

Sarah A. Witzgall

Table of Contents

Page

List of Figures

Page

List of Tables

Page

TENSION-TENSION FATIGUE BEHAVIOR OF NEXTEL 720 ALUMINA/MULLITE AT 1200°C IN LABORATORY AIR AND IN STEAM

I. Introduction

A composite is a type of material that consists of two or more phases made up of different constituent materials, that when these materials act together, they exhibit more favorable properties than if they were to act alone. Typically, one of the phases is discontinuous and stronger, known as the reinforcement. The less stiff and weaker phase is typically continuous and is called the matrix; an illustration of this is shown in Figure 1. Depending on the application and type of composite, each of the phases plays a different role. In high-performance structural composites, the continuous fiber reinforcement takes most of the load and determines its strength from the direction of the fibers. In these types of materials, the matrix phase provides support and protection for the sensitive fibers and the local stress transfer from one fiber to another [1].

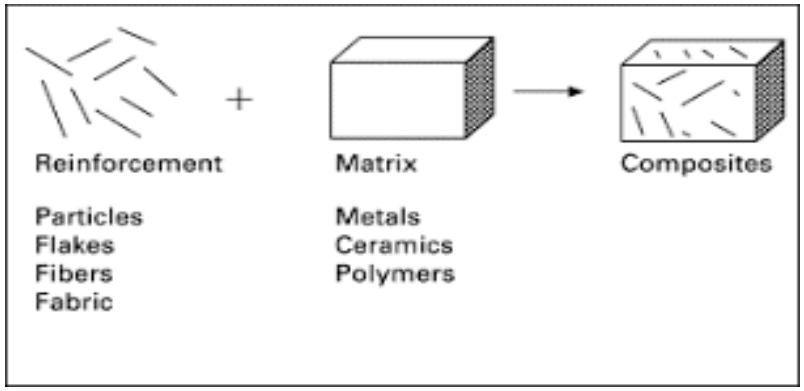

Figure 1. Illustration of the reinforcement and matrix phases forming a composite material [2]

Composite materials have been used increasingly in different applications across the world for centuries. One of the first uses of composite materials can date back to 1500 B.C., where early Egyptians used straw, a reinforcement, and a mixture of clay, sand, and water, a matrix, to create strong, durable buildings [3]. In the 1930s, organic resins were developed along with the first synthetic fibers, which opened up the world of fiber-reinforced composites. During the second half of the 20th century, fiber-reinforced composites started to develop and become competition for more traditional materials such as metal and ceramics [4].

Today, composite materials have become the dominant material used in the aerospace industry. They have become the baseline for all other materials' properties to base on due to their low-weight, high-strength defining properties. They were first introduced into military aircraft in the 1960s, since then each generation of aircraft have seen an increase in the number of composite materials used in production. Composites are often the first choice for structural elements due to their weight-saving capabilities. To go higher and further, aircraft need to be able to have the strength and rigidity to support the loads, which is why composites are a great choice since more weight typically limits performance [4].

Composite materials are expanding from just being used primarily in structural components of aircraft, but also are beginning to be used in engine applications. Ceramic matrix composites (CMCs) are the particular type of composite being explored for these engine applications.

According to a 2018 report by Stratview Research, the CMC market is one of the fastest-growing markets in the aviation industry, and the use of CMC material and

component used in aircraft was projected to double from 2018 to 2023. The report states that “CMCs are as tough as metals and are just one-third the weight of nickel alloys and can operate at 1,300° Celsius. They have the ability to withstand extreme temperatures and require less cooling air to be diverted from the thrust. As of result, engines run at higher thrust” [5].

A current example of CMCs being used in aircraft can be found in the U.S. Air Force’s F-16 Fighting Falcon. In the F-16’s engine, the exhaust nozzle has five A500 ceramic matrix composite divergent seals, which are identified by the yellow arrows in Figure 2 [6].

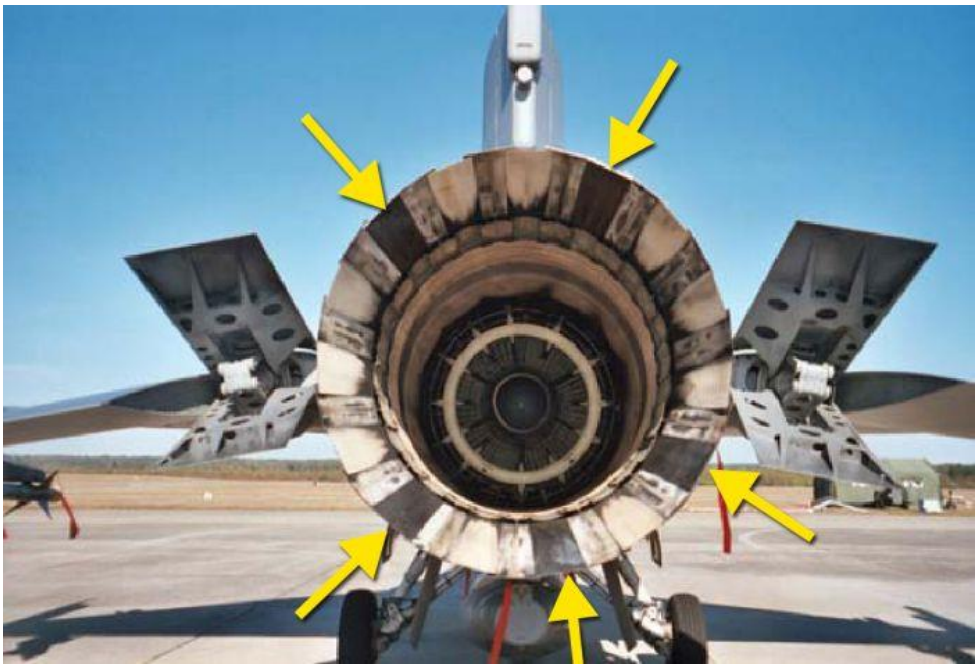

Figure 2. F-16 Fighting Falcon engine exhaust nozzle with five CMC seals shown with yellow seals. Photo courtesy of U.S. Air Force. [6]

This study is based on the effect on tension-tension fatigue behavior of NEXTEL™720/alumina-mullite ceramic matrix composite at 1200°C in laboratory air and steam environment. The objective is to determine the effect that steam and maximum stress level have on the fatigue behavior of the N720/AM composites.

II. Literature Review

2.1 Composites

A composite material is one that combines two or more components that may differ in chemistry or structure to combine their properties into more superior material. The constituent materials retain their chemical, physical, and mechanical properties when combined. Therefore they do not combine chemically with one another, which differs significantly from metallic alloys [7]. Composite materials consist of a combination of materials that are mixed to create a product with specific structural properties to enhance the strength, ductility, or whatever other characteristics are needed for the application. Typical composite materials consist of strong and stiff fibers made of glass, carbon, fiberglass, and embedded in a matrix made of epoxy or thermoplastic polymer material [8].

Composite materials offer many advantages. The main benefits of using a composite material are their high strength and stiffness and low density when compared to bulk materials. Using a composite offers a weight reduction in the final product when a bulk material is replaced with a composite material [7]. Composite materials are also becoming more critical for the construction of aerospace structures. During the 1960s, composite materials were beginning to be developed for use in aircraft for their weight savings over traditional aluminum parts. Newer generation larger aircraft are currently designed with all-composite fuselage and wing structures [8].

Additionally, bulk materials, such as metals and polymers, are typically considered isotropic materials. Therefore, the material properties are not considered to vary with direction. However, composite materials are typically treated as anisotropic materials.

Anisotropic materials have properties that vary with the direction within the material. Composite materials are mostly considered orthotropic, a sub-class of anisotropic materials. Orthotropic materials have properties that are different in three mutually perpendicular directions and axes. Therefore, the loads that are loaded parallel to these axes will produce just normal strain, but if not loaded in parallel, the loads will produce both normal and shear strains. This means that orthotropic mechanical properties are a function of orientation [7].

Composites can be manufactured in many different ways. The way a composite is manufactured is very dependent on what the material will be used for and what types of properties it should possess to accomplish its goal. There are four different classifications of composite materials: fibrous composite materials, laminated composite materials, particulate composite materials, and combinations of some or all of the previous three. Laminated composite materials consist of layers of composite materials sandwiched and bonded together. Particulate composite materials are where particles of different shapes and sizes are embedded into a matrix material. The short fibers used in particulate composites are known as whiskers and have the same near-crystal sized diameter as the longer fibers. Fibrous composite materials consist of long, strong, and stiff fibers. Fibers are characterized by their high length-to-diameter ratio. Due to their characteristics, fibers are typically stronger and stiffer than their bulk form. These fibers are oriented in a specific direction or are embedded into a softer material, known as the matrix. Matrix materials are usually polymers, but metals, carbons, and composites are also used. The three major classes of polymers are thermoplastic, thermosets, and rubbers, and are based on the method of fabrication. Metal matrix composites are made

by pouring molten metal around an in-place fiber system using diffusion bonding or other heating methods. Ceramic matrix composites are discussed in detail in Section 2.3 [9].

2.2 Ceramics

A ceramic material can be defined as inorganic materials that are constituted by the combination of metallic and non-metallic elements whose properties depend on the way the elements are linked. Ceramics may be the most versatile branch of materials, due to their chemical nature. The bonds in ceramic materials are mostly strong ionic and covalent bonds present in different proportions. These bonds help determine the properties of ceramics, such as high fusion temperatures, high wear strength, and low ductility [10].

There are two different categories of ceramics: traditional and advanced ceramics. Traditional ceramics are based on silicates and typically made with natural raw materials; some examples are cement and clay products. Advanced ceramics are manufactured by more advanced methods with artificial raw materials that have undergone distinct treatments to achieve higher purity. These types of ceramics are carbides, pure oxides, and borides [10].

Ceramic materials have many applications due to their vast and unique properties based on their composition and how they were manufactured. However, one of the main issues with monolithic ceramics is their inherent brittleness, as well as their catastrophic failure mode that can lead to low damage tolerance under service conditions [11]. A way to take advantage of the high-temperature properties of ceramics and overcoming the brittleness of ceramics is through ceramic matrix composites [12].

2.3 Ceramic Matrix Composites

In the 21st century, there is a strong need to develop new stronger, tougher, and better materials to meet the needs and challenges of new applications. Ceramic matrix composites (CMCs) are among a group of materials that were identified as a potential material to improve the thrust-to-weight ratio of high-performance aircraft engines. Engineers in the United States, Europe, and Japan have been considering CMCs and using CMCs in gas turbine engines. Besides the high-temperature capabilities, CMCs also offer a weight reduction compared to traditional materials used in engines [13]. CMCs are potential candidates due to their excellent physical and mechanical properties. CMCs are heterogeneous materials where a second phase is embedded into the ceramic matrix. CMCs can combine high strength, hardness, and temperature stability with different properties based on the nature of their reinforcing phase [14].

Some CMCs have a unique ability to repair themselves through self-healing cracks [14]. Being self-healing is the capability of a system to repair damage by itself, so its cracks are sealed. A self-healing system should be able to repair damage more than once so that as new cracks appear, they can be repaired as well. This type of approach is ideal for aerospace applications as it would allow for longer lifetimes and increased sustainability among parts with these features. Self-healing can occur inside or on the outer surface of CMCs. Also, using CMCs can potentially improve damage tolerance by incorporating reinforcement phases into the ceramic matrix. This enhances the fracture toughness of the material [11].

2.3.1 Non-Oxide CMCs

Non-oxide CMCs have great potential and are currently more widely used in high-temperature applications than other types of composites. Particular non-oxide CMCs such as C/SiC and SiC/SiC composites show high thermal conductivity, excellent thermal shock stability, creep and oxidation resistance, and improved toughness compared to the monolithic material [11]. C/SiC composites inherit the exceptional properties of their fibers and matrix while overcoming the brittleness of typical monolithic ceramics [15].

Silicon carbide composites are fabricated using chemical vapor or liquid phase infiltration of matrix material into a preform prepared from the silicon carbide fibers. These types of composites are used in combustors, shrouds of gas turbine engines, and heat exchangers [16].

Cracks exist in all-ceramic materials, including CMCs, and are typically caused by either processing or created by an applied mechanical or thermal load. Especially at high temperatures in moist oxidizing environments, cracks can allow oxygen diffusion within the material, which aggravates chemical degradation. To prevent oxidation behavior, a glassy oxide phase can be used to fill voids and cracks within the material. The oxide is typically added as a protective coating, but it can also be formed by the oxidation of non-oxide compounds within the coating or the bulk of the material. When it is in the bulk of the material, the undergoing oxidation acts as a chemical fuse against additional oxidation. Self-healing can remain efficient in these composites if the oxide remains chemically and thermally stable [11].

Not all CMCs are self-healing, and the biggest weakness of non-oxide composites is the oxidation they experience when exposed to oxidizing environments such as air and

steam. To combat this problem, non-oxide composites typically need an environmental barrier as a coating [12].

2.3.2 Oxide-Oxide CMCs

Oxide-oxide CMCs are a highly sought-after material for many different applications, especially those in the aerospace industry. Advanced engine designs call for an increase in turbine engine temperatures. Higher temperatures allow for higher power, efficiency, and can help reduce emissions in the air. Oxide-oxide composites are made up of an oxide fiber and an oxide matrix. Since both the fiber and the matrix are composed of oxide materials, these types of composites do not oxidize when exposed to environments such as air and steam. Therefore, oxide-oxide composites are a great candidate for these types of applications due to inherent oxidation resistance and provided damage tolerance from either a weak fiber/matrix interphase or their porous matrix [17].

Typically, oxide fibers are considered to have lower strength and creep resistance than covalently bonded materials such as SiC found in non-oxide CMCs. However, in the mid-1990s, two new fibers, NEXTEL™ 620 fiber, and NEXTEL™ 720 fiber, were developed that have a uniquely high tensile strength and creep resistance for oxide fibers. Additionally, these fibers are entirely crystalline and do not contain silica, such as previous NEXTEL™ fibers [18].

Specifically, the creep resistance of the NEXTEL™ 720 fiber allowed for the fabrication of an oxidation-stable ceramic composite with a useful load-bearing capability

above 1000°C. This superior performance results from a high content of mullite in the fiber, which has a better creep resistance than alumina [18].

Oxide-oxide CMCs have shown excellent stability in ambient air when tested at elevated temperatures. Additionally, there have been several studies that evaluated the effects of different environments on the properties of oxide-oxide CMCs. In many applications, porous-matrix oxide-oxide CMCs are exposed to high temperatures, high pressures, and salt fog or excessive moisture. Oxide-oxide CMCs are also used in applications where they may be subject to fatigue loading. The effects of frequency and environment on fatigue behavior of different oxide-oxide materials has taken place. Previously, the focus has been on N720/A. The research found that the loading frequency has little effect on fatigue performance at 1200°C in air. However, it was concluded that not only did steam have an impact on the lifetimes of the material, but frequencies also dramatically impacted fatigue life [17]. This is why more research is incredibly important for oxide-oxide materials to expand further the knowledge of what impact environment, frequency, and other factors play into lifetimes of these materials.

2.4 Fatigue Testing

Fatigue is defined as the progressive, localized, permanent structural change that occurs when a material is subjected to fluctuating stresses and strains that may result in cracks or fractures after a sufficient number of fluctuations. Fatigue cracks initiate and propagate in regions where the strain is most severe [19].

Tension-tension fatigue indicates the stress is cycled between a maximum and minimum tensile stress. The stress ratio is the algebraic ratio of the minimum stress to the

maximum stress. In tension-tension fatigue, the stress ratio becomes a positive number less than 1.

2.5 Previous Research Efforts

Previous research has been performed on NEXTEL™720/alumina (N720/A) and NEXTEL™720/alumina-mullite (N720/AM) ceramic composites at the Air Force Institute of Technology. In 2008, Genelin [18] studied the effects of creep on N720/AM with 0°/90° fiber orientation at 1200°C in air, steam, and argon environments. His results show that the N720/AM composite showed both primary and secondary creep regimes in both air and steam. Larger creep strains were accumulated in the steam environment. Genelin reported that the specimens in the steam environment displayed heavily-reduced creep lifetimes. Additionally, his work in the argon environment provided evidence that the argon had a negative effect on the creep performance of the N720/AM [20].

In 2010, Ozer studied N720/AM with 45-degree fibers in a creep environment at 1200°C in air, steam, and argon environments. Ozer examined tensile creep behavior for creep stresses in the 13-32 MPa. He observed primary and secondary creep regimes in all tests. In this testing, creep run-out was defined as 100 h and was achieved at 20 MPa. Additionally, the air results showed longer lifetimes than specimens tested in steam and in argon at the same stress levels. It was concluded that matrix degradation was the cause of early failures in the argon and steam tests [21].

Also, in 2010, Kutsal studied the effects of the steam environment on creep behavior of N720/AM at elevated temperatures of 900°C, 1000°C, and 1100°C. Kutsal found increasing creep strains with an increase in test temperature. Kutsal noted in his

creep-rupture tests that the creep accumulation remained low for the N720/AM tests in air at all temperatures but remained higher than the creep accumulation for the previous testing accomplished on N720/A. Kutsal's research concluded that steam caused larger creep strains, and higher stress levels decreased the creep life of N720/AM [22].

2.6 NEXTEL™720/Alumina-Mullite

The N720/AM is an oxide-oxide ceramic matrix composite, which consists of NEXTEL^{TM}720 fibers and a porous alumina-mullite matrix. The oxide matrix is composed of mullite and alumina particles in a sol-gel derived alumina. The content of mullite in the matrix composition is approximately 12.5 % (by volume). There is no interface between fiber and matrix, and the material relies on the porous matrix for damage tolerance. The NEXTEL™720 fiber is manufactured by Minnesota Mining and Manufacturing Company (3M) [23]. The NEXTEL™720 fiber, composed of 85 wt.% Al_2O_3 and 15 wt.% SiO_2, was developed for load-bearing applications at temperatures above 1000°C. The superior high temperature creep performance of NEXTEL™/720 fiber results from a high content of mullite, which has much better creep resistance than alumina. Volume calculations indicate that mullite comprises about 55% of the fiber volume. The high content of mullite lowers the fiber density by about 13% and its thermal expansion coefficient by about 0% [18].

2.7 Thesis Objective

The objective of this research was to assess the tension-tension fatigue behavior of the N720/AM ceramic matrix composite at 1200°C in laboratory air and steam. Multiple tests were conducted in both environments at varying maximum stress levels. Elevated-

temperature fatigue behavior of this composite has not been studied previously. Therefore, experimental investigation of the tension-tension fatigue response of this composite at elevated temperature in laboratory air and steam will provide necessary knowledge about its thermo-mechanical performance. Additionally, the ability to compare the CMC behavior under cyclic (fatigue) loading researched in this work and that under sustained loading (creep) researched in previous studies [20]–[22] will help determine which type of loading history is more damaging for this material. Furthermore, a comparison of the results of this work with those previously reported for the NEXTEL™720/alumina CMC will help determine whether the addition of mullite to the composite matrix is beneficial.

III. Methodology

3.1 Chapter Overview

This chapter explains the details of the testing and equipment used to perform this research. Additionally, detailed descriptions of all test procedures and microstructural analyses are provided.

3.2 Mechanical Testing Equipment

The mechanical testing equipment used was an 810 Material Test System (MTS), a servo-hydraulic testing machine fitted with MTS water-cooled hydraulic wedge grips. The machine, shown in Figure 3, has a load cell of 5-kip capacity. In all tests, the grip pressure was set to 8 MPa. During testing, the grips were cooled to 15°C using a Neslab RTE 7 chiller. An MTS FlexTest 40 digital controller and MTS Multipurpose Testware (MPT) software were used to program test routines and collect test data.

Figure 3. Test Station with 5-kip MTS and accompanying equipment

Since all tests were performed at an elevated temperature of 1200°C, the testing machine was equipped with an Amteco two-zone furnace. The furnace contained two heating elements per zone and was insulated with Rescor 310M foam composed of over 99% pure fused silica and rated up to 1648°C. The foam was cut and baked out to fit the specimen, susceptor, and extensometer without interfering with the heating elements. An internal view of one side of the furnace is shown in Figure 4. The two heating elements are enclosed in the 310M foam, and a thermocouple is placed through a hole in the top of the 310M foam on each side. An MTS 409.83 Temperature Controller was used to control the temperature of the furnace surrounding the specimen during testing. The MTS Controller used two R-type thermocouples to regulate and maintain the temperature throughout the test.

Figure 4. Internal View of Amteco Furnace

To measure strain, a high-temperature extensometer from MTS (Model 632.53E-14) with a gauge section of 12.5 mm was used. The data from the extensometer is displayed in the MTS software. Due to the nature of the material, the specimens were not marked with extensometer indentations; preferably, the extensometer was just placed against the material. The extensometer is shown in Figure 5.

Figure 5. MTS Extensometer

3.3 Procedures and Processes

3.3.1 Material and Test Specimen

The oxide-oxide composite studied in this work was NEXTEL™720/ alumina-mullite (N720/AM. This CMC consists of NEXTEL™720 fibers and a porous matrix comprised of alumina and mullite particles in a sol-gel derived alumina. The content of mullite in the matrix composition is approximately 12.5 % (by volume). The composite was fabricated by COI Ceramics (San Diego, CA). The composite was supplied in the form of a 3.2-mm thick plate, consisting of 12 0°/90° woven layers, with a density of ~2.63 g/cm^3 and a fiber volume of approximately 40.4%. Composite porosity was ~26.8%. The fabrication procedure is described in Ref [24]. The composite has no

coating applied to the fibers and relies on the porous matrix for damage tolerance. The overall microstructure of the CMC is shown in Figure 6, showing 0° and 90° fiber tows, as well as multiple matrix cracks formed during material synthesis.

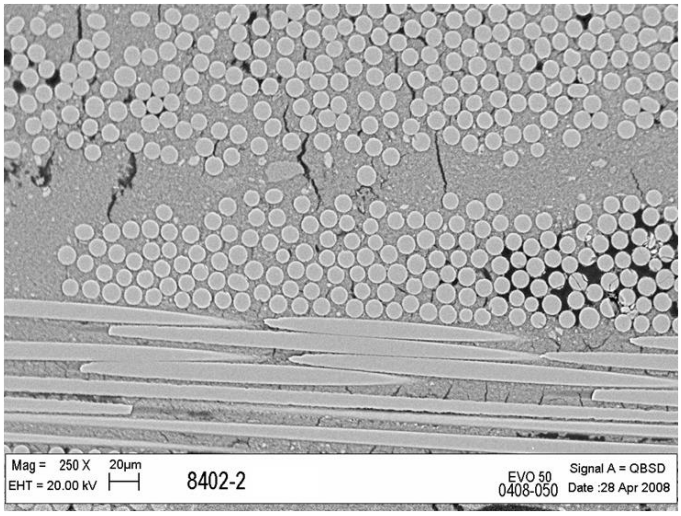

Figure 6. Typical microstructure of the N720/AM ceramic composite. Micrograph courtesy of A. Szweda, COI Ceramics Inc. [24]

Standard dogbone-shaped specimens shown in Fig. 6 were used in all tests. The test specimens were machined using diamond grinding at the AFIT model and fabrication shop. After machining, the specimens were cleaned by soaking in deionized water for 20 min, followed by soaking in ethyl alcohol for an additional 20 min. The specimens were then dried in an oven for 2 h at 250°C.

Upon examination of the as-processed panel, it was noticed that a portion of the panel was warped. Consequently, some of the test specimens were not flat. When a bent specimen is gripped in a properly aligned testing system, it is immediately subjected to a bending moment. Hence when testing bent material, it is understood that the test

specimen is subjected to a combination of tension and bending. It is furthermore expected that such a specimen will fail prematurely. Due to the short supply of costly experimental material, the bent specimens were tested despite the aforementioned considerations.

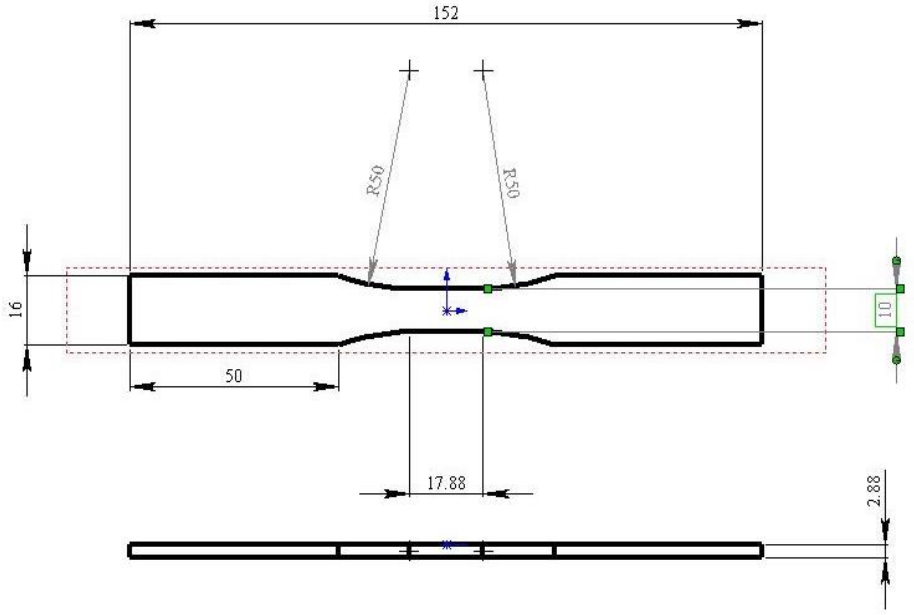

Figure 7. Test specimen, dimensions in mm.

Prior to testing, fiberglass tabs were attached to the gripping sections on both sides of each test specimen using M Bond 200 adhesive. The tabs help prevent potential damage to the specimen caused by the wedge grips of the MTS machine. A specimen equipped with tabs is shown in Figure 8.

Figure 8. Specimen equipped with tabs and ready for testing

The width and thickness of each specimen gauge section were measured using a Mitutoyo Corporation digital micrometer (shown in Figure 9) at least three times. The average of these values was recorded for each specimen. These values are essential for determining the specimen's cross-sectional area, which is used in engineering stress calculations.

Figure 9. Mitutoyo Corporation Digital Micrometer

During testing, an alumina susceptor is placed around the specimen. The susceptor has openings for the steam pipe, extensometer, and the specimen. The susceptor is shown in Figure 10 below, with labels indicating each opening.

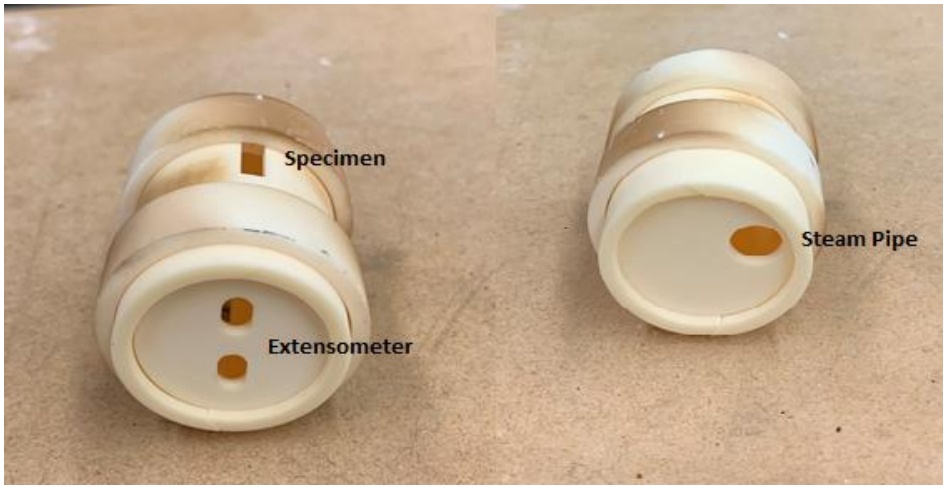

Figure 10. Susceptor (front and back views) used in all tests

3.3.2 Temperature Calibration

All tests were performed at a temperature of 1200°C. One specimen was used for temperature calibration. This specimen was instrumented with two R-type thermocouples. The thermocouples were placed on the specimen in the test section, and then scrap pieces of N720 Alumina were placed over the thermocouples to help keep the thermocouples in the proper spot on the specimen. To hold everything in place, piano wire was wrapped around the specimen. This ensured the thermocouples would not slip off the specimen during calibration. The calibration specimen was placed in the susceptor during testing, and the same external insulation was used that would be used during a standard test. This ensures the most accurate calibration for subsequent tests. The temperature calibration specimen with the thermocouples attached is shown in Figure 11.

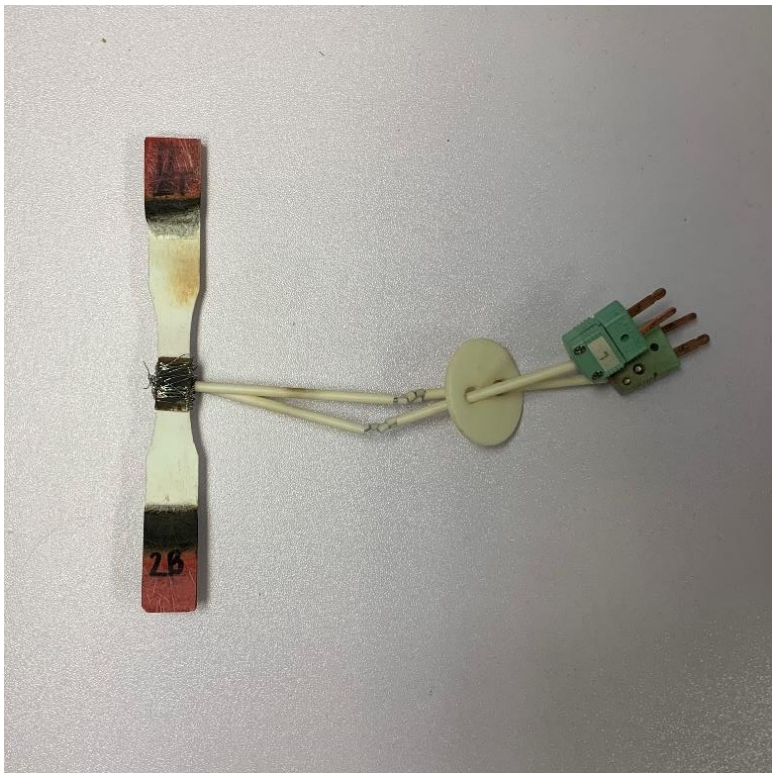

Figure 11. A test specimen instrumented with thermocouples for temperature calibration

The specimen was first placed in the top grip and gripped applying a 0 N force under force control. Switching to displacement control, the lower grip was moved upward until it surrounded the bottom grip section of the specimen. The control mode was switched to force control, where it was set to zero, and the bottom grip was quickly closed. The furnace was closed and locked around the sample with the thermocouples hanging out. A small piece of insulation was also placed on the top of the oven. In Figure 12, the experimental set-up for temperature calibration is shown. The insulation is shown on top of the furnace, as well as the thermocouples hanging from the specimen.

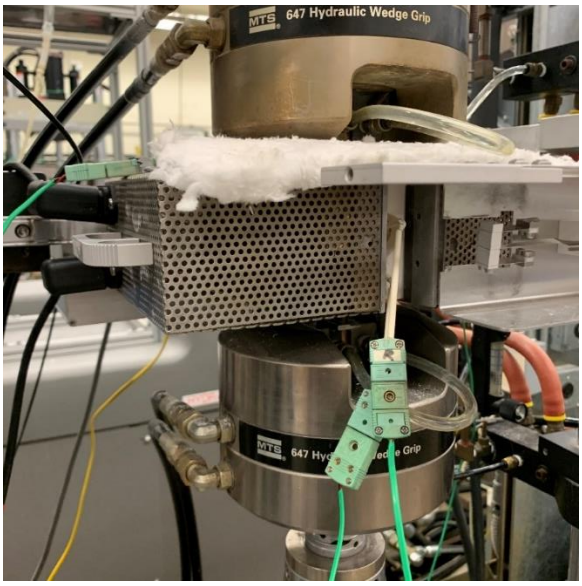

Figure 12. Experimental Set-up for Temperature Calibration

When this specimen was placed in the furnace, the specimen temperature reading was collected via an external Omega Type-R Thermometer (Figure 13) and recorded.

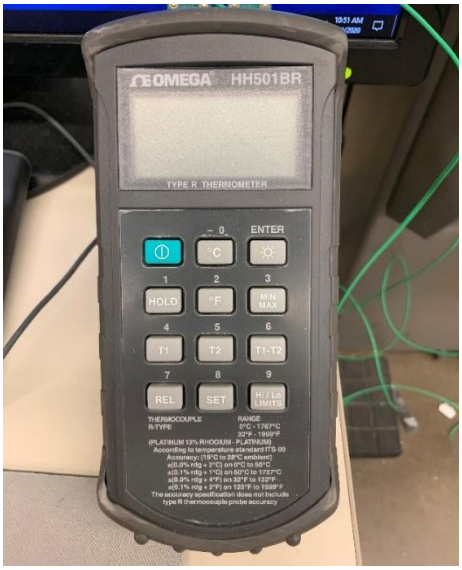

Figure 13. Omega Type-R Thermometer

The setpoints on the temperature controller for the left and right furnace zones were increased incrementally until the temperature on both sides of the specimen was within ±5°C of the desired temperature of 1200°C. At this point, the temperature controller settings were held constant for one hour to ensure that the specimen temperature remained at 1200±5°C. Temperature calibration was performed separately for both laboratory air and steam tests. When any heating elements or internal insulation needed to be replaced, the temperature calibration was repeated, and the temperature controller settings adjusted to ensure all tests were performed at the target temperature of 1200°C.

3.3.3 Fatigue Testing

Tension-tension fatigue tests were conducted in force control at 1200° in laboratory air and in steam. For testing, the specimen was placed into the alumina susceptor and loaded into the wedge grips of the machine. The furnace was closed and secured around the specimen, and the external insulation was placed on top of the furnace. When testing in the steam environment, the steam is manually turned on and warmed up for 50 min before beginning the rest of the test procedure. The specimen is heated to the set temperature at a rate of 1°C/s, then held at test temperature for 60 min. All fatigue tests were performed with a ratio of minimum to maximum stress of 0.1 at 1 Hz. Fatigue run-out was defined as 100,000 cycles.

Throughout each test, strain, force, displacement, force command, cycle number, and left/right temperature data were recorded using the MPT software. Data was collected for each portion of the test: warm-up, cyclic loading, tension to failure for the specimens that achieved fatigue run-out. The warm-up data shows the strain and

temperature during the warm-up and dwell periods. From this data, the thermal strain can be determined. During the fatigue portion of the test history, two types of data files are recorded. First, peak-valley data for each cycle is recorded. For each peak and valley, the following data were collected: strain, force, displacement, force command, cycle number, and left/right temperature) were recorded. Additionally, full-cycle data (data collected at various time intervals throughout a given cycle such that a cyclic stress/strain hysteresis loop can be constructed) was collected for cycles 1-10, every 10^{th} cycle between cycles 10 and 100, every 100^{th} cycle between cycles 100 and 1000, every 1000^{th} cycle between cycles 1000 and 10000 and every 10000^{th} cycle between cycles 10000 and 100000. The full cycle data also include strain, force, displacement, force command, cycle number, and left/right temperature. Specimens that achieved run-out in fatigue tests were unloaded to zero force and then subjected to a tensile test to failure to evaluate the retained properties.

If, at any point during the test, a furnace element failed, leading to a lower than the desired temperature, the test program would command unloading to zero force and shut off the furnace. Next, the specimen would be removed from the testing machine and inspected for damage. The furnace elements would be replaced, and a temperature calibration would be accomplished for the newly installed elements. The setpoints for the temperature controller would be changed in the MPT software to ensure testing at the target temperature of 1200°C. The specimen would then be reloaded into the testing machine, and testing would resume.

The testing facility used in this research exhibited malfunction during this experimental effort. The furnace used in this work employs four heating elements (two in

each heating zone). In several tests, one or more heating elements failed part-way through the test. The test had to be interrupted, and the specimen cooled down to room temperature to permit replacement of the heating element(s) followed by temperature calibration. Then the test was restarted. Unusually frequent failures of the heating elements pointed to a larger problem with the furnace/temperature controller system. Finally, the testing was halted to determine the underlying cause of the increasingly frequent failures of the heating elements. It was determined that the electrical system connecting the MTS controller to the furnace elements was faulty. The entire electrical system was replaced prior to testing in steam. Following the replacement of the electrical system, the issues with the heating elements ceased. Additionally, the specimens tested after the electrical system was replaced produced significantly longer cyclic lives. Because all testing in air was accomplished before the electrical system was replaced, the lower cyclic lives obtained in air are likely due to the malfunctions of the electrical system. Once again, we note that the fatigue tests performed in steam after the electrical system was replaced produced significantly longer cyclic lives.

3.3.4 Monotonic Tension Testing

Tension tests to failure at 1200°C for this composite were previously performed and reported by Genelin [22]. Due to a limited number of test specimens' tension to failure, tests were not repeated in this effort. Instead, tensile properties previously reported by Genelin [22] were used to design the fatigue test matrix as well to assess the retention of tensile strength in the specimens that survived 100,000 fatigue cycles. Genelin reported the following average tensile properties for the N720/AM composite at 1200°C: the

ultimate tensile strength (UTS) of 153.2 MPa, the elastic modulus of 74.5 GPa, and the failure strain of 0.34%. Tensile stress-strain curves obtained by Genelin [22] are reproduced in Fig. 14 for readers' convenience.

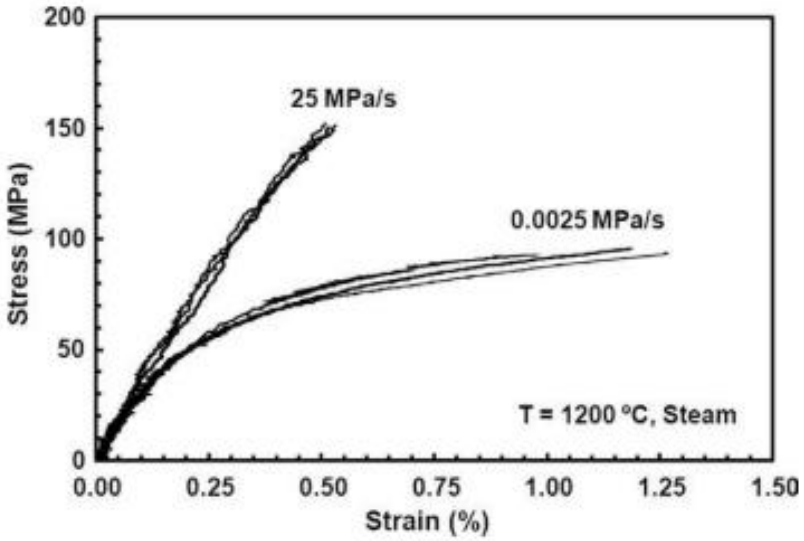

Figure 14. Tensile stress-strain curves N720/AM obtained in tests conducted with loading rates of 0.0025 and 25 MPa/s at 1200°C in steam. Figure reproduced from Genelin. [25]

However, the N720/AM specimens used in this research were cut from a different panel and therefore had a different fiber volume fraction than those tested by Genelin [22]. His research used samples that were cut out of a panel with a fiber volume fraction of 40.4% [25]. The composite studied this research had a fiber volume fraction of 38.5%, while the CMC tested by Genelin had the fiber volume fraction of 40.4%. Therefore, the UTS reported by Genelin [22] is adjusted for the V_f = 38.5% using the following equation,

$$UTS_{adj} = \left(\frac{40.4}{38.5}\right) * UTS$$

The adjusted UTS is found to be 160.8 MPa. Likewise, the modulus of elasticity reported by Genelin [22] is adjusted for the V_f = 38.5% according to the following equation,

$$E_{adj} = \left(\frac{40.4}{38.5}\right) * E$$

The adjusted modulus of elasticity is found to be 78.2 GPa. The adjusted modulus and UTS values are used to assess the retained tensile properties of the pre-fatigued specimens.

3.3.5 Microstructural Characterization

The first step in microstructural characterization is examining the specimens under the optical microscope. The optical microscope used was a Zeiss Discovery V12 and is shown in Figure 15. Photos were taken of all four sides (front, back, left, right) of the two halves of each failed specimen. Under normal operating conditions, the examination of the failed specimens with an optical microscope would be followed with the examination of the fracture surfaces using a scanning electron microscope (SEM). Unfortunately, due to the shut-down caused by the COVID-19 pandemic, we did not have access to an SEM and were not able to accomplish this important part of the microstructural investigation. Hence it is recommended that the fracture surfaces produced in this work be examined with an SEM in the future when regular operation is resumed.

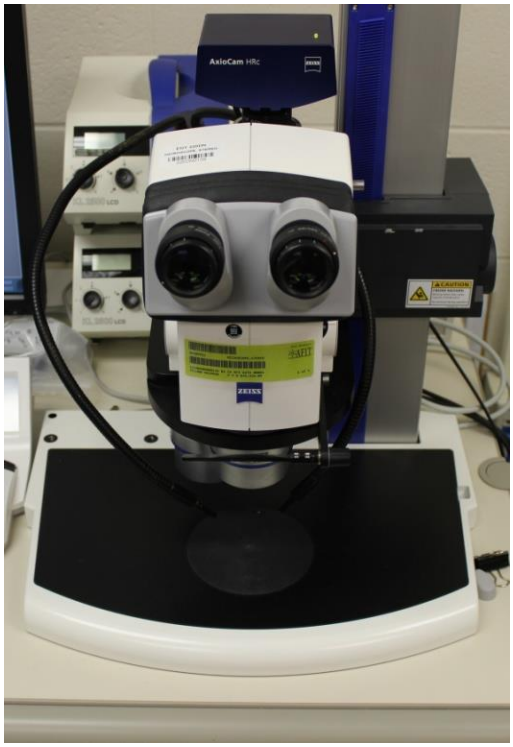

Figure 15. Zeiss Discovery V12 optical microscope equipped with an AxioCam HRc digital camera

IV. Results and Discussion

4.1 Thermal Expansion of N720/AM at 1200°C

The coefficient of thermal expansion was determined from strain and temperature data collected during the warm-up portion of the test. The coefficient of thermal expansion was calculated using the following equation,

$$\alpha = \frac{\varepsilon}{\Delta T}$$

Where ε is the thermal strain measured after the warm-up and initial dwell at test temperature was complete, and ΔT is the difference between the ambient temperature of the laboratory environment (24°C) and the test temperature (1200°C). In this work, the representative thermal strain was 0.72%, and the calculated coefficient of thermal expansion, 6.15×10^{-6}/K. This value agrees reasonably well with the average coefficients of thermal expansion of 6.45×10^{-6}/K and 7.09×10^{-6}/K reported by Genelin [20] and Ozer [26], respectively.

4.2 Tension-Tension Fatigue Results

Tension-tension fatigue tests were conducted at a frequency of 1.0 Hz with a sinusoidal waveform at 1200°C in laboratory air and steam. The ratio of the minimum stress to the maximum stress was R = 0.1. The maximum stress levels ranged from 45 MPa to 136 MPa. For these tests, fatigue run-out was defined as 1×10^5 cycles. This run-out condition is consistent with previous AFIT research for comparison purposes. The results of the tension-tension fatigue tests are shown in Table 1. The results are also displayed in Figure 16 as maximum stress versus cycles to failure (S-N) curves.

Table 1. Summary of tension-tension fatigue results obtained for N720/AM composite at 1200°C in laboratory air and steam

Specimen	Test Environment	Maximum Stress (MPa)	Maximum Stress (%UTS)	Cycles to Failure (N)
07	Laboratory Air	136	84.5	7886
06	Laboratory Air	92	57.2	24894
05	Laboratory Air	60	37.3	11209
04	Laboratory Air	60	37.3	70616
09	Laboratory Air	45	30.0	100696[a]
10	Steam	136	84.5	20212
15	Steam	120	74.6	100000[a]
11	Steam	92	57.2	70306
13	Steam	92	57.2	100000[a]
12	Steam	60	37.3	180000[a]
14	Steam	60	37.3	100000[a]

[a] Run-out. Failure of the specimen did not occur when the test was terminated.

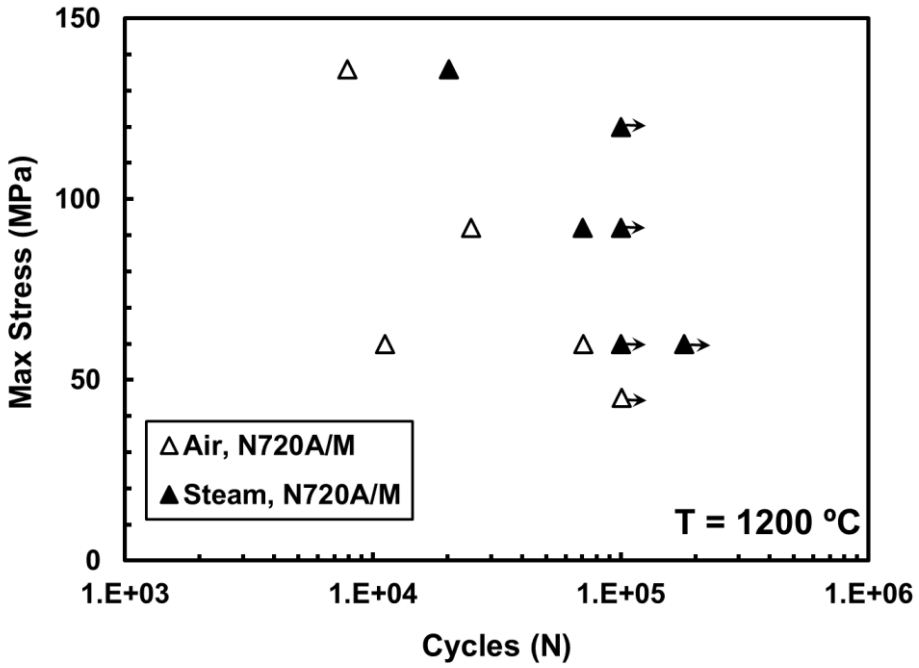

Figure 16. Stress vs. cycles to failure for N720/AM at 1200°C in laboratory air and steam. The arrows indicate that failure of the specimen did not occur when the test was terminated

As shown in Figure 16, the fatigue life decreases with increasing maximum stress. The fatigue lives obtained in steam are longer than those obtained in air. However, as stated earlier, this unexpected result is most likely due to problems with the test material and specimens and with the electrical system of the test set-up. As noted earlier in Section 3.3.3, some of the test specimens were bent prior to testing and thus were subjected to a combination of tension and bending during tension-tension fatigue tests. Such a combination of tensile and bending loads is considerably more damaging than tensile load alone and is expected to result in premature failure of the test specimen. Additionally, as pointed out in Section 3.3.3, the electrical system of the test set-up exhibited persistent malfunction during testing in air. Subsequently, the electrical system was replaced after the first steam test of 136 MPa, and no malfunctions occurred during the remainder of the steam testing. Hence, we believe that shorter cyclic lives produced in air do not necessarily indicate that air environment is more damaging to this composite compared to the steam environment. Moreover, we recommend that fatigue tests in air be repeated to produce more reliable results.

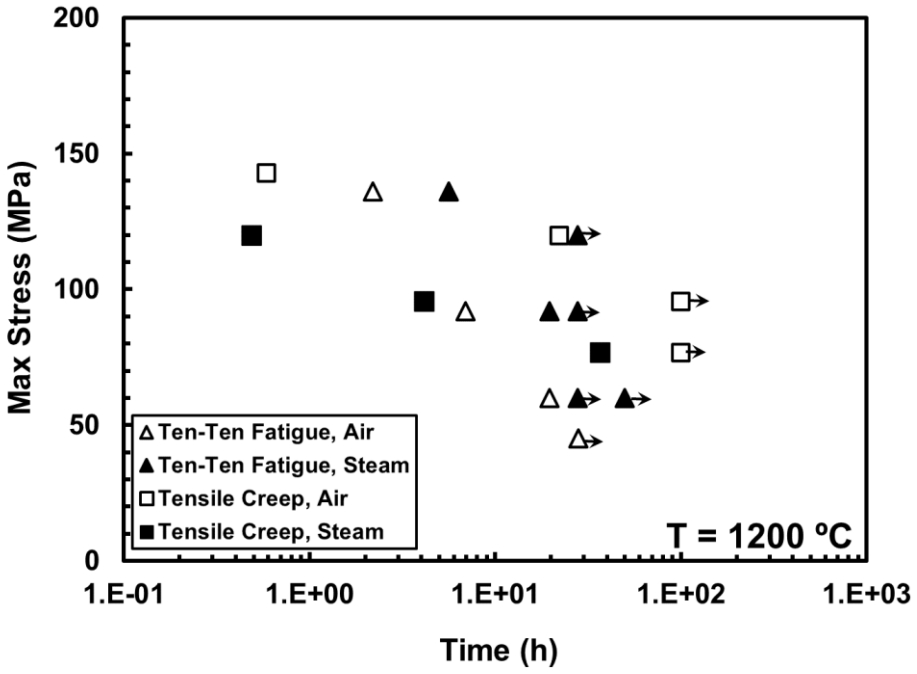

Figure 17. Stress vs. time to failure for N720/AM at 1200°C in laboratory air and steam obtained in tension-tension fatigue and in tensile creep. The arrows indicate that failure of the specimen did not occur when the test was terminated. Creep-rupture data from Genelin [22]. All data are adjusted for Vf = 0.385.

The lifetimes of the specimens tested in tension-tension fatigue were also compared to creep lifetimes obtained for this material in previous work [22] in Figure 16. Note that creep run-out was defined as 100 h, whereas tension-tension fatigue run-out was defined as 100,000 cycles or 27.7 h. The tensile creep run-out in air was achieved at 77 MPa and 95 MPa. However, creep run-out was not achieved in steam. The longest creep lifetime produced in steam was 37 h at creep stress level of 77 MPa. However, this 37-h creep lifetime still exceeds the lifetime defined as run-out for the tension-tension fatigue tests. In the tension-tension fatigue tests, run-out was achieved at 45 MPa in the air environment and at 120, 92, and 60 MPa in the steam environment. Due to the difficulties

with the test material and the electrical system described above, the tension-tension fatigue results obtained in air are inconclusive. It is our strong recommendation that additional tension-tension fatigue tests in air be accomplished.

More conclusions can be drawn from the test results produced in steam. In tension-tension fatigue, the specimens were able to achieve run-out at 120 MPa. At the same stress level under tensile creep loading, the test did not even last a full hour with the specimen failing after a mere 0.49 h. Additionally, the specimen tested in creep at 95 MPa failed after only 4.18 h, whereas the specimen tested in fatigue achieved a run-out (corresponding to a lifetime > 27.7 h) at 90 MPa. A conclusion can be drawn that at 1200°C in steam creep is much more damaging to N720/AM than tension-tension fatigue.

When analyzing composite response under cyclic loading, it is important to consider the change in the composite modulus (hysteresis modulus determined from the maximum and minimum stress-strain data points during a load cycle). Noticeable decrease in modulus with cycles indicates damage development, more specifically pointing to the damage done to the load-bearing fibers [23]. The change in normalized modulus (i.e., modulus normalized by the modulus obtained on the first cycle) with fatigue cycles at 1200°C is shown in Figure 18 (air and steam) and in Figure 19 (steam only). The steam test with the maximum stress of 136 MPa was performed before the correction of the electrical issue. There appears to have been an increase in the damage after a fatigue crack was potentially initiated. The same type of pattern can be seen in some of the air tests, particularly in the 136 MPa fatigue test. However, a decrease in the normalized modulus is slightly more pronounced in steam. However, we cannot make any conclusions on if steam accelerates damage development occurring during fatigue

cycling. More testing needs to occur, especially in the air environment, in order to make more conclusive remarks on the normalized modulus trends seen in this test effort.

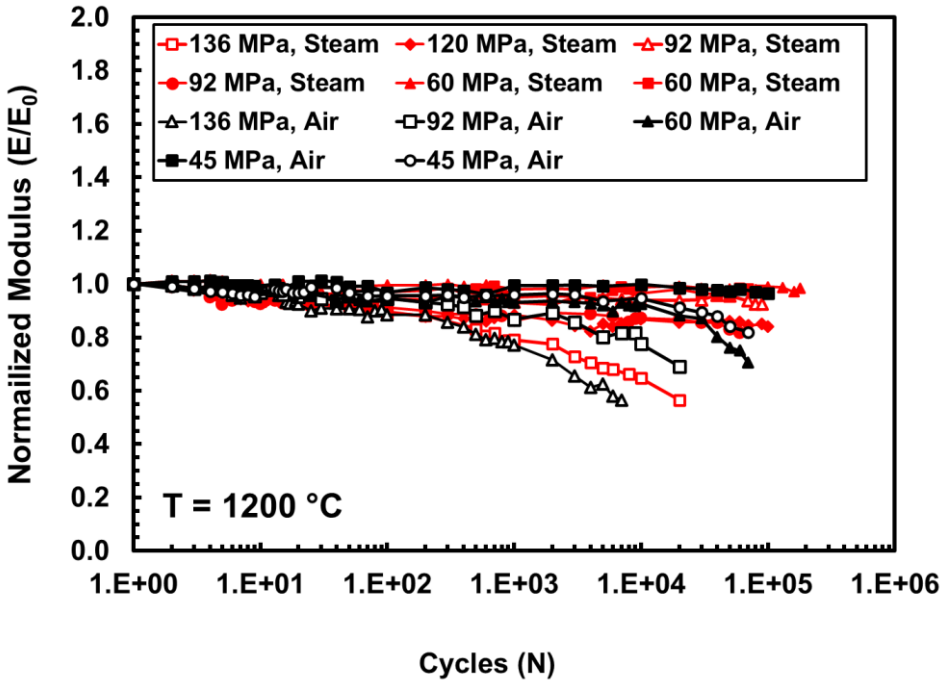

Figure 18. Normalized modulus vs. cycles for N720/AM at 1200°C in air and steam

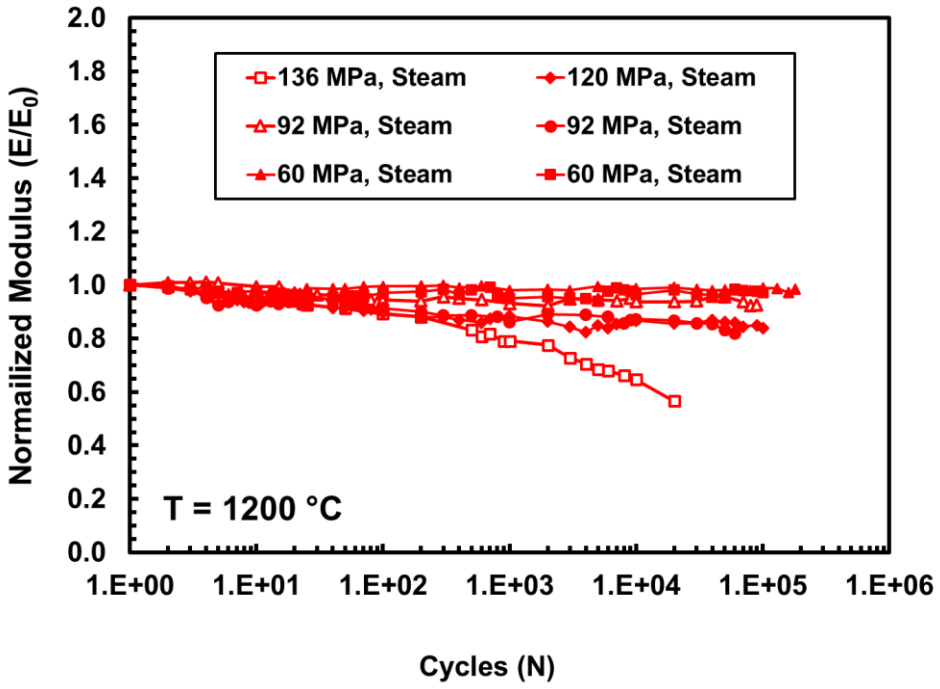

Figure 19. Normalized modulus vs. cycles for N720/AM at 1200°C in steam

Strain accumulation (i.e. strain measured at the completion of a cycle) vs. fatigue cycles is shown in Figure 20 (air and steam) and in Figure 21 (steam only). In these figures, little strain accumulation is seen at the beginning of the tests. However, later in the test, progressive strain accumulation occurs in all tests. Strain ratcheting (viz. strain progressive strain accumulation with cycles) is more dramatic in tests performed with the higher stress levels, for example, the 120 MPa in steam and 136 MPa tests in both steam and in air. The specimen, which achieved fatigue run-out at 120 MPa in steam, still shows strong strain accumulation toward the end of the test. In this case, strain ratcheting is likely due to progressive matrix cracking. The specimen tested at 136 MPa in steam did not achieve run-out. In this test, there is a sharper increase in strain accumulation before the specimen failure (Figure 21).

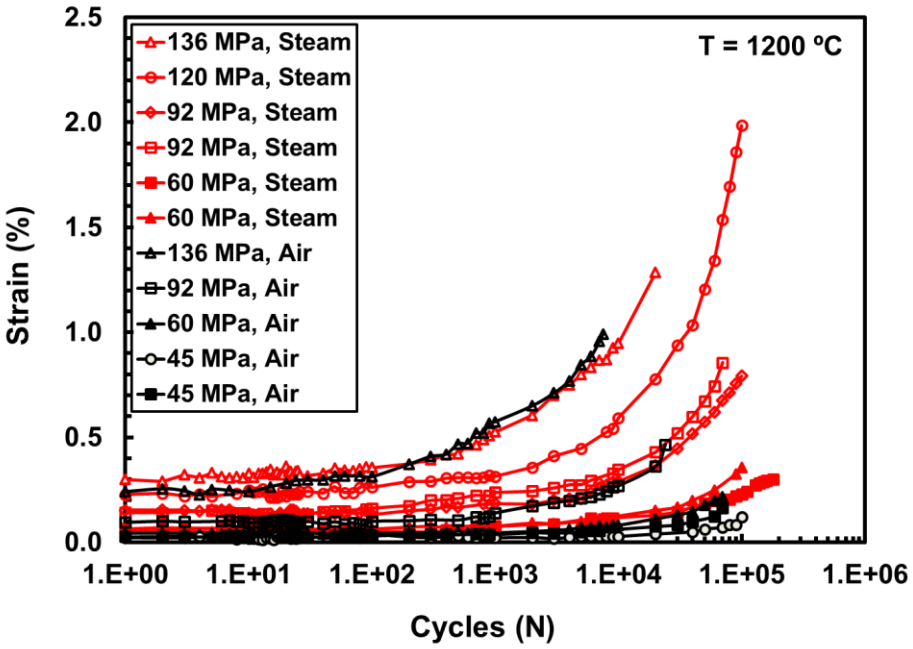

Figure 20. Strain accumulations (%) vs. cycles (N) for N720/AM at 1200°C in air and steam

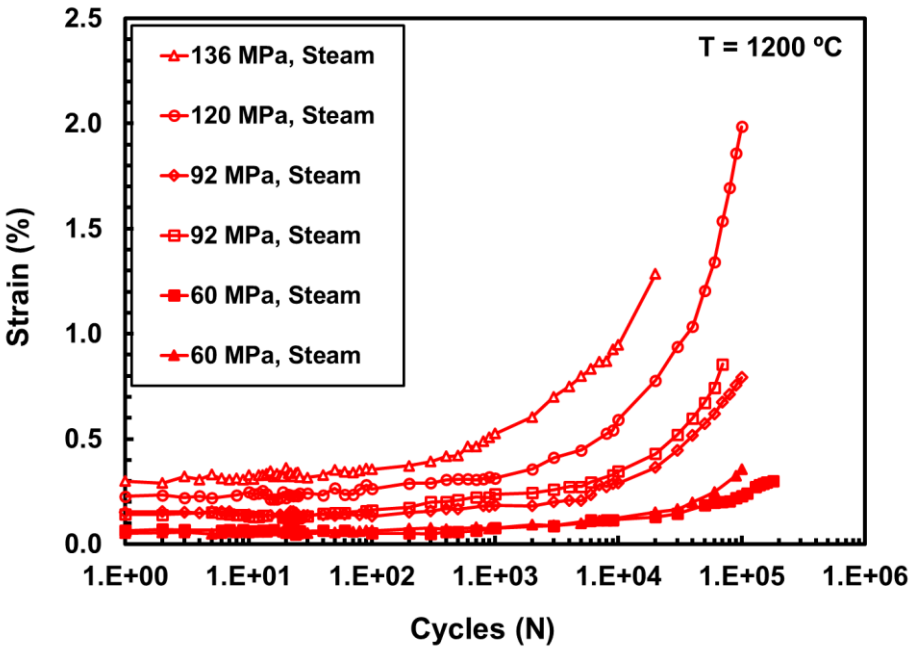

Figure 21. Strain accumulations (%) vs. cycles (N) for N720/AM at 1200°C in steam

4.3 Effects of Steam on Tension-Tension Fatigue

Due to the malfunction of the electric system in the test set-up described in Section 3.3.3, it is difficult to draw reliable conclusions regarding the effects of steam on fatigue performance of N720/AM at 1200°C. A comparison of the fatigue data obtained in steam to the creep data obtained in steam in prior work [22] suggests that N70/AM shows promising material behavior under tension-tension fatigue. The cyclic lifetimes exceed the creep lifetimes obtained under similar maximum stresses in steam. Since in tension-tension fatigue, the specimens were able to achieve run-out at 120 MPa and at the same stress level, the creep test did not even last a full hour with the specimen failing after a mere 0.49 h. From this, it is concluded that the sustained creep load is more damaging to N720/AM than fatigue is in the steam environment.

4.4 Retained Tensile Strength

All specimens that achieved the fatigue run-out of $1x10^5$ cycles were tested in tension to failure at 1200°C to assess the retained tensile strength. During this research effort, one specimen achieved fatigue run-out in air, and four specimens achieved fatigue run-out in steam. These specimens were subjected to a tension test to determine the retained tensile strength. Evaluation of retained strength is useful in gaging the degree of damage caused to the composite by prior fatigue loading. The retained tensile properties are summarized in Table 2 and in Figure 21. Recall that the adjusted UTS for this composite was found to be 160.8 MPa.

Table 2. Retained tensile strength of N720/AM specimens subjected to prior fatigue at 1200°C in laboratory air and in steam

Fatigue Stress (MPa)	Test Environment	Retained Strength (MPa)	Strength Retention (%)
45	Air	172.69	100
120	Steam	143.97	90
92	Steam	168.70	100
60	Steam	147.36	92
60	Steam	159.16	99

All N720/AM specimens subjected to prior fatigue at 1200°C in air or in steam retained a high percentage of their tensile strength. Strength retention was relatively independent of the test environment, ranging between 90% and 100%. The average retained strength for the specimens tested in steam is excellent at 95%. One specimen tested at a maximum stress of 45 MPa achieved fatigue run-out in air retained 100% of its tensile strength. Potentially, the 45 MPa stress level was low enough to not have any damage development in the fibers.

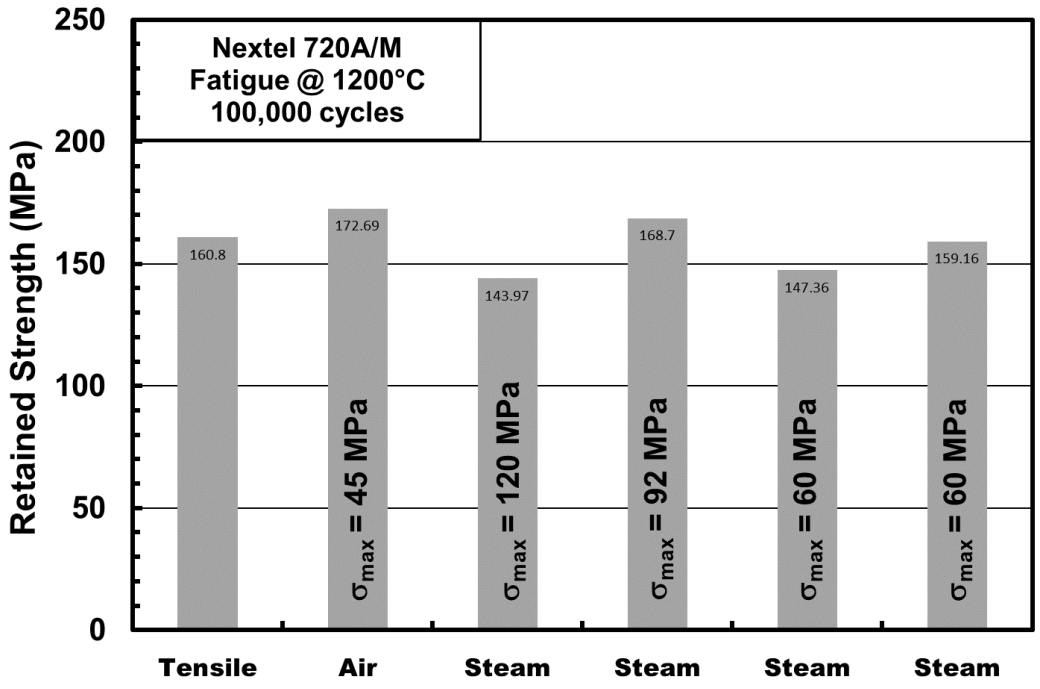

Figure 22. Retained tensile strength of N720/AM specimens subjected to prior fatigue in air and steam at 1200°C

4.5 Composite Microstructure

As loading continues, damage builds up as individual fibers break and matrix cracks form. When individual fibers break, the load is re-distributed among the surviving fibers. The failed specimens were examined under an optical microscope. As mentioned earlier in the manuscript, we were unable to examine the failed specimens under a scanning electron microscope due to the shut-down caused by the COVID-19 pandemic. Yet an SEM examination is needed to form a complete picture of the damage and failure mechanisms operating in the composite. Hence, we strongly recommend that the fracture surfaces produced in this work be examined under an SEM when the shut-down restrictions are lifted.

Optical micrographs of the failed N720/AM specimens are presented in Figure 24 - Figure 27. When reviewing optical micrographs, we pay special attention to the size of the damaged section and the type of failure (brushy vs. planar). Most of the failed specimens exhibit brushy (or fibrous) fracture surfaces where fiber pull-out is clearly visible. The specimens tested at the higher stress levels tend to have longer damage zones and more pronounced fiber pull-out. The specimens tested with lower stress levels also show fiber pull-out, but the damage zones are shorter than those produced at the higher stress levels. However, even with the differences in the damage zones, there is no apparent correlation between the size of the damage zone and the fatigue stress level. Additionally, the test environment appears to have little effect on the fracture surface topography. The fracture surfaces obtained in steam are similar to those obtained in air. Greater insight into the influence of maximum stress test environment on the fracture surface topography and the microstructure of N720/AM specimens could be gained by examining the fracture surfaces under an SEM. Such examination is strongly recommended for future work.

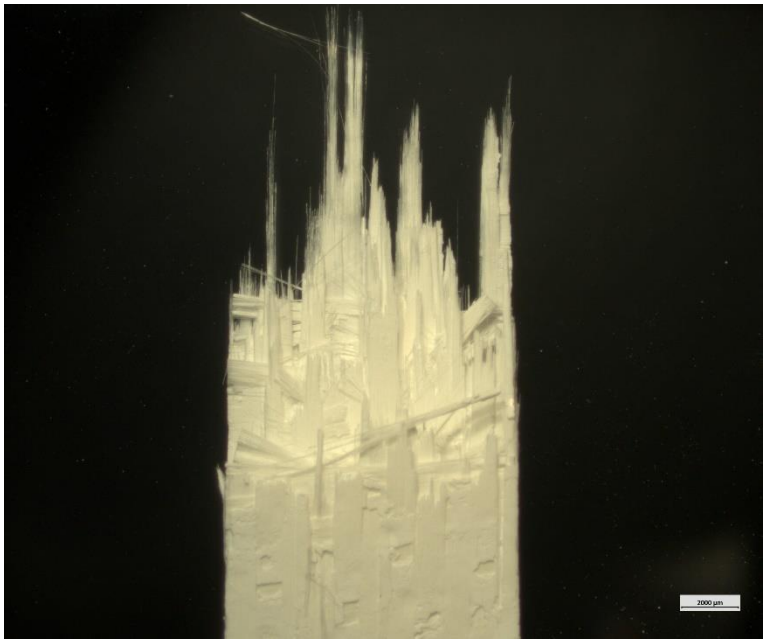

Figure 23. Optical micrograph of the fracture surface of N720/AM specimen tested in tension-tension fatigue at 1200°C in air. σ_{max} = 136 MPa, N_f = 7886.

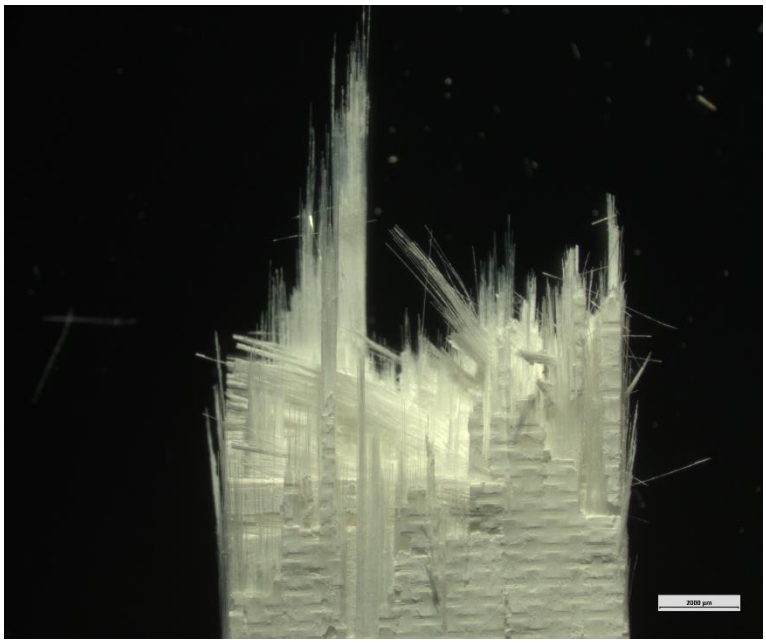

Figure 24. Optical micrograph of the fracture surface of N720/AM specimen tested in tension-tension fatigue at 1200°C in steam. σ_{max} = 120 MPa, N_f > 100000.

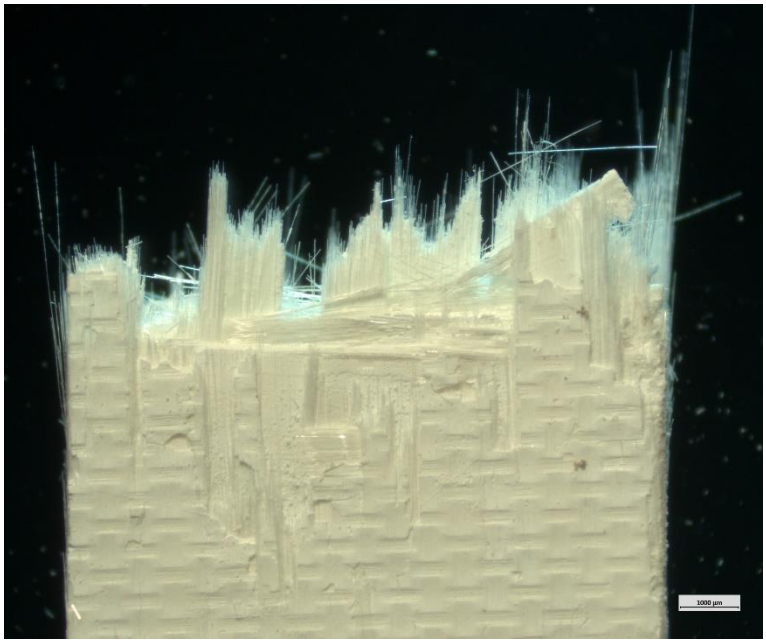

Figure 25. Optical micrograph of the fracture surface of N720/AM specimen tested in tension-tension fatigue at 1200°C in steam. σ_{max} = 92 MPa, N_f > 100000.

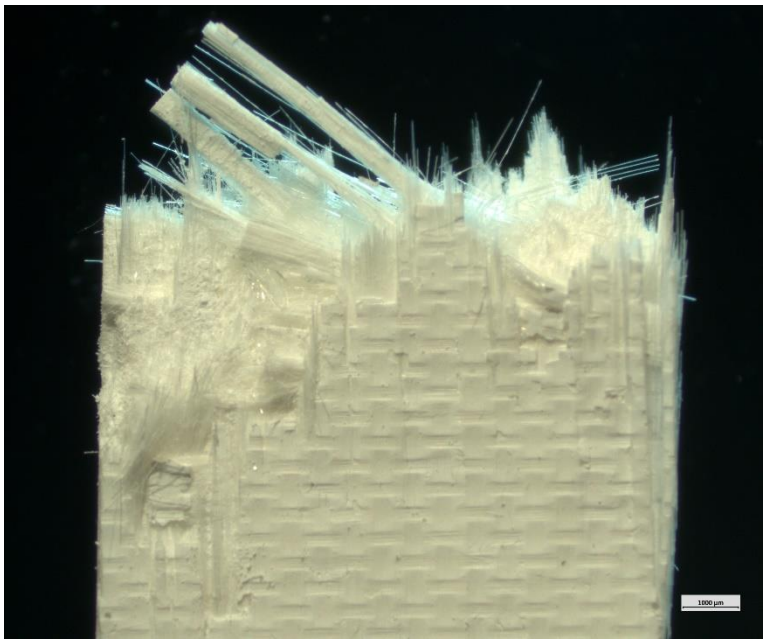

Figure 26. Optical micrograph of the fracture surface of N720/AM specimen tested in tension-tension fatigue at 1200°C in steam. σ_{max} = 60 MPa, N_f > 100000.

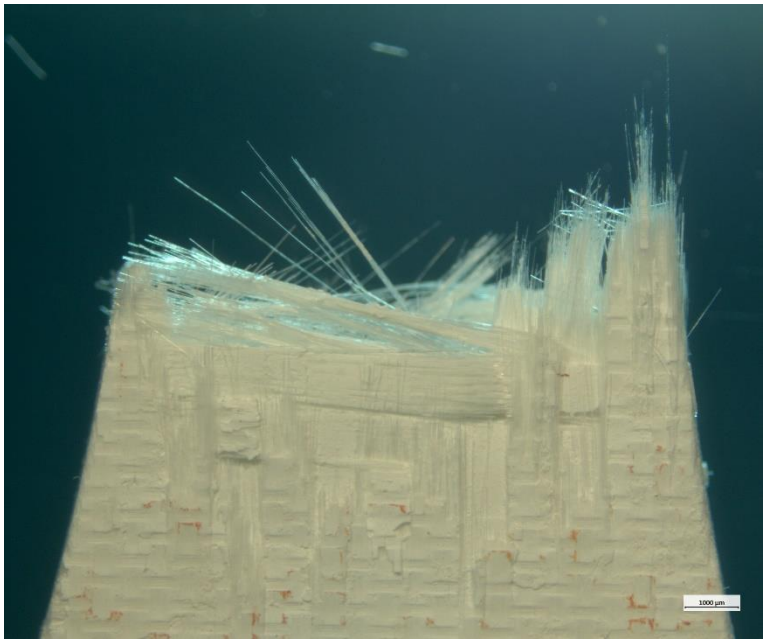

Figure 27. Optical micrograph of the fracture surface of N720/AM specimen tested in tension-tension fatigue at 1200°C in air. σ_{max} = 45 MPa, N_f > 100000.

V. Conclusions and Recommendations

5.1 Conclusions

The tension-tension fatigue behavior of N720/AM composite material was investigated at a loading frequency of 1.0 Hz, at 1200°C in laboratory air and steam. The ratio of minimum to maximum stress was R = 0.1. Fatigue stress levels ranged from 45 MPa to 136 MPa in laboratory air and from 60 MPa to 136 MPa in steam. Fatigue run-out was defined as 100,000 cycles. Fatigue run-out was achieved at 45 MPa in laboratory air and at 120 MPa in steam. Due to difficulties with the test material (some specimens appeared bent) and the electrical system of the test set-up experienced at the beginning of this effort, the results obtained in air are somewhat inconclusive. Hence we cannot reliably assess the effect of steam environment on the fatigue performance of this composite at 1200°C. However, we are able to compare the steam tests that were performed after the correction of the set-up to previous research done by Genelin. There was no creep run-out in the steam environment. Comparing this to the fatigue run-out accomplished at 120 MPa, we can conclude that creep is more damaging to N720/AM than fatigue is in the steam environment.

All specimens that achieved run-out were tested in tension to failure to assess the retention of tensile strength. Most pre-fatigued specimens retained over 95% of their tensile strength. In one case, lower strength retention of 90% was observed. Excellent strength retention indicates that no significant damage occurred to the load-bearing fibers during fatigue cycling.

The N720/AM fracture surfaces produced in fatigue tests at 1200°C appear to be dominated by regions of fibrous fracture with visible fiber pull-out. The fracture surface appearance cannot be directly correlated with the cyclic life. Neither does the test environment appear to influence the fracture surface topography strongly. Similar fracture surfaces are obtained in steam and in air. However, it is recognized that we must examine the fracture surfaces under an SEM in order to reach accurate conclusions pertaining to the composite microstructure.

5.2 Recommendations

Due to the limited number of test specimens and the difficulties with both test material and the test set-up described earlier in the manuscript; we strongly recommend that experimental investigation of the fatigue behavior of this composite be continued. In order to gain further confidence in the findings of this research, more specimens should be tested in tension-tension fatigue in both laboratory air and steam. Additionally, the failed specimens should be examined under a scanning electron microscope to gain a better understanding of the damage and failure mechanisms operating in the composite subjected to cyclic loading at 1200°C in air and in steam.

Appendix. Composite Micrographs

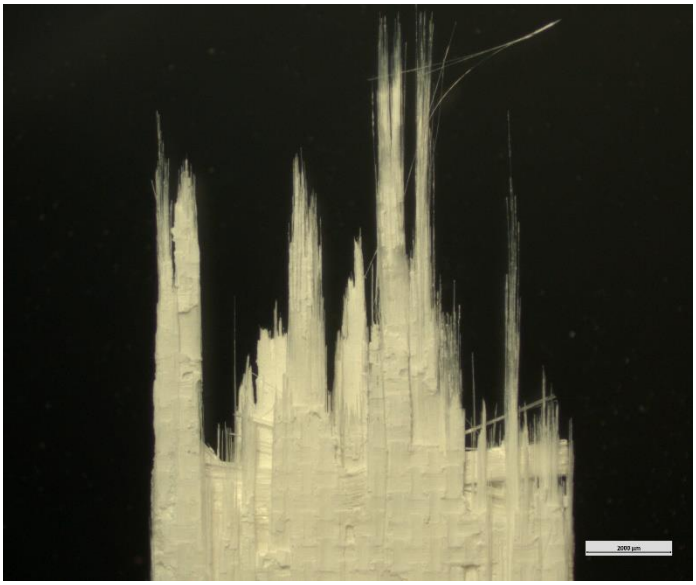

Figure 28. Optical micrograph of the fracture surface of N720/AM specimen tested in tension-tension fatigue at 1200°C in air. σ_{max} = 136 MPa, N_f = 7886.

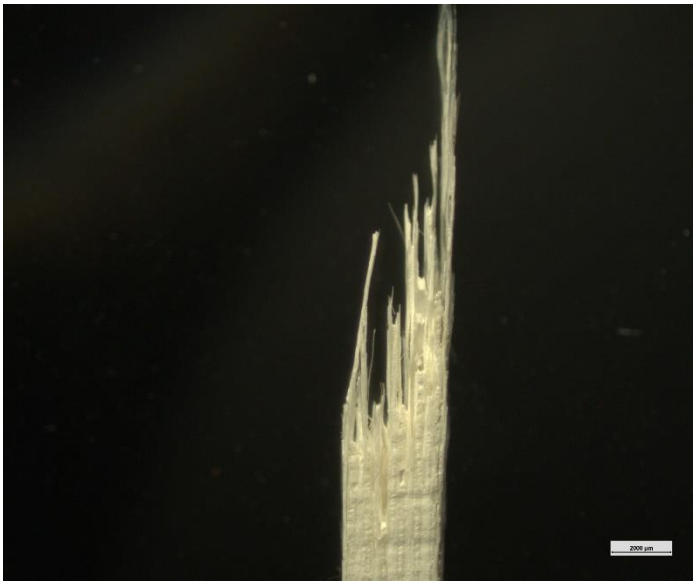

Figure 29. Optical micrograph of the fracture surface of N720/AM specimen tested in tension-tension fatigue at 1200°C in air. σ_{max} = 136 MPa, N_f = 7886.

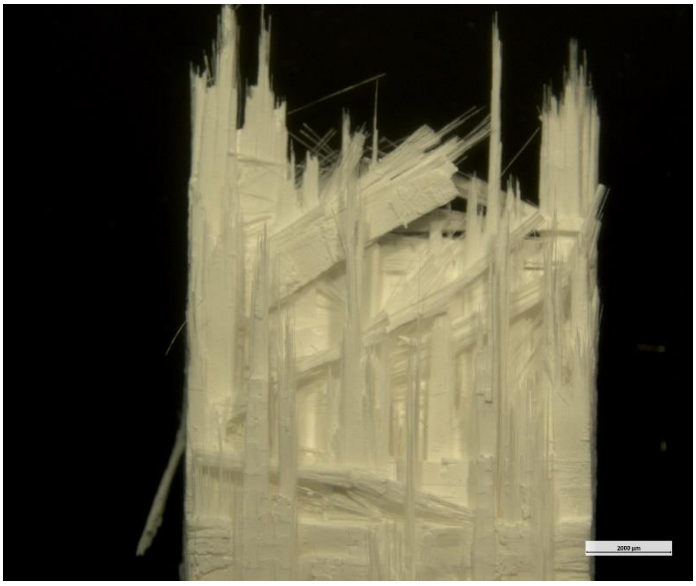

Figure 30. Optical micrograph of the fracture surface of N720/AM specimen tested in tension-tension fatigue at 1200°C in air. σ_{max} = 136 MPa, N_f = 7886.

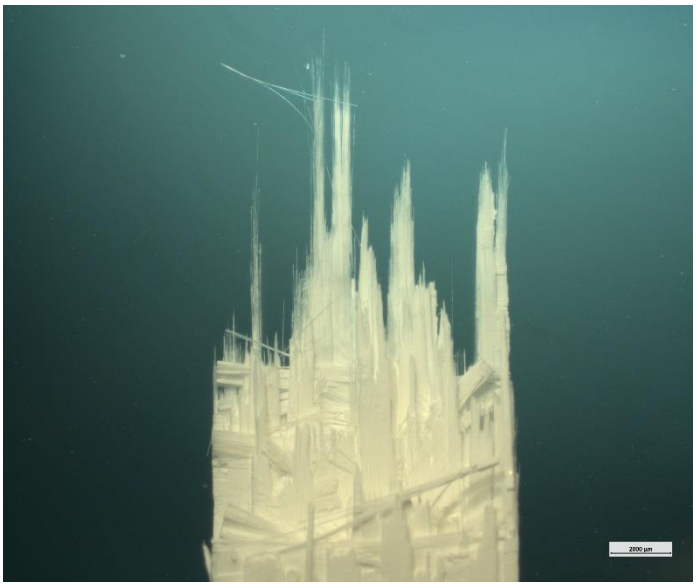

Figure 31. Optical micrograph of the fracture surface of N720/AM specimen tested in tension-tension fatigue at 1200°C in air. σ_{max} = 136 MPa, N_f = 7886.

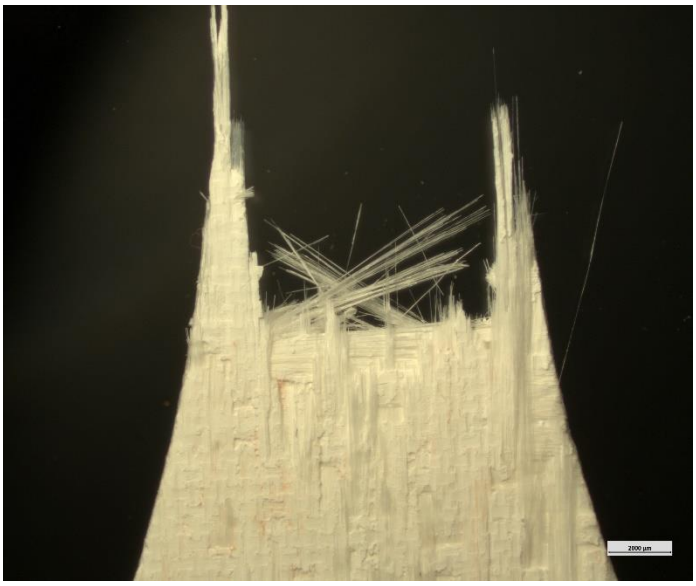

Figure 32. Optical micrograph of the fracture surface of N720/AM specimen tested in tension-tension fatigue at 1200°C in air. σ_{max} = 92 MPa, N_f = 24894.

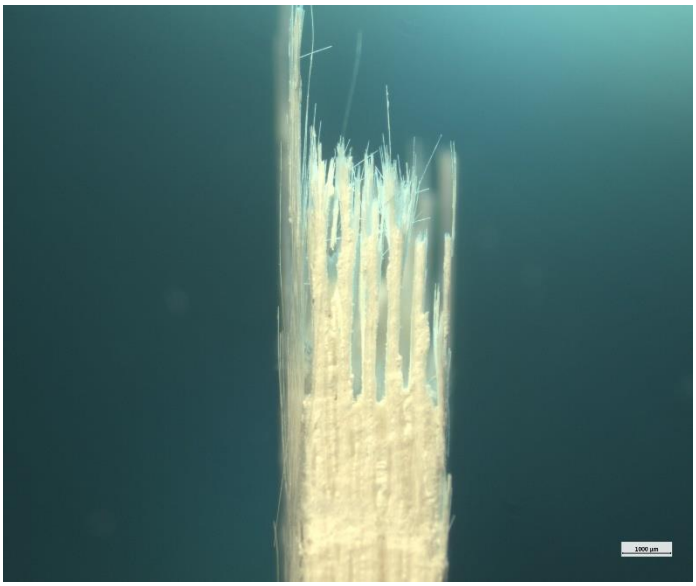

Figure 33. Optical micrograph of the fracture surface of N720/AM specimen tested in tension-tension fatigue at 1200°C in air. σ_{max} = 92 MPa, N_f = 24894.

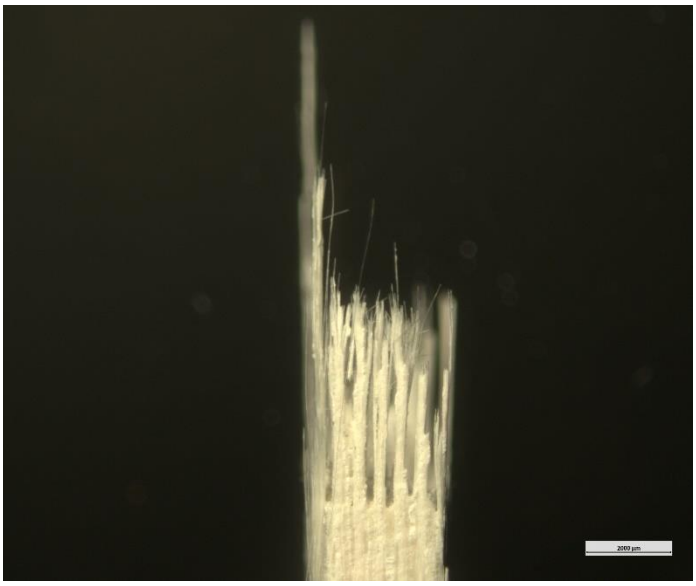

Figure 34. Optical micrograph of the fracture surface of N720/AM specimen tested in tension-tension fatigue at 1200°C in air. σ_{max} = 92 MPa, N_f = 24894.

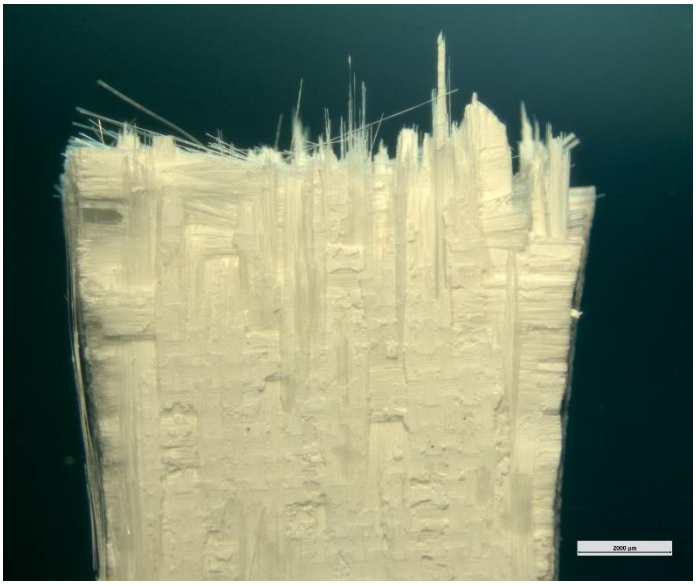

Figure 35. Optical micrograph of the fracture surface of N720/AM specimen tested in tension-tension fatigue at 1200°C in air. σ_{max} = 92 MPa, N_f = 24894.

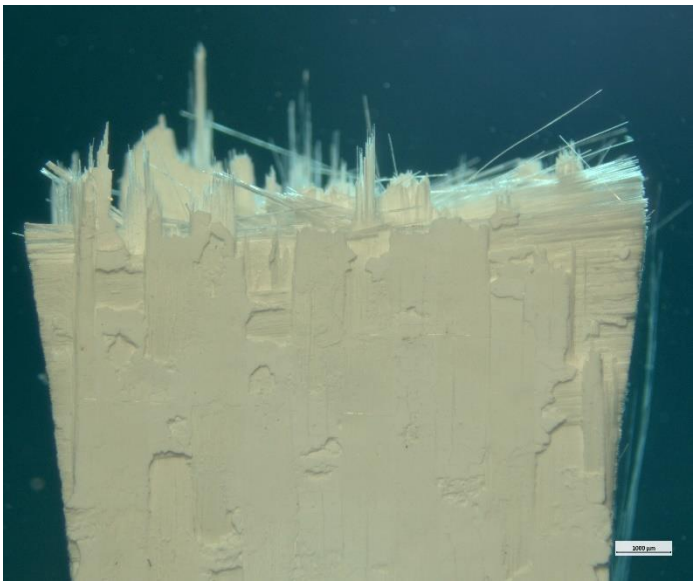

Figure 36. Optical micrograph of the fracture surface of N720/AM specimen tested in tension-tension fatigue at 1200°C in air. σ_{max} = 92 MPa, N_f = 24894.

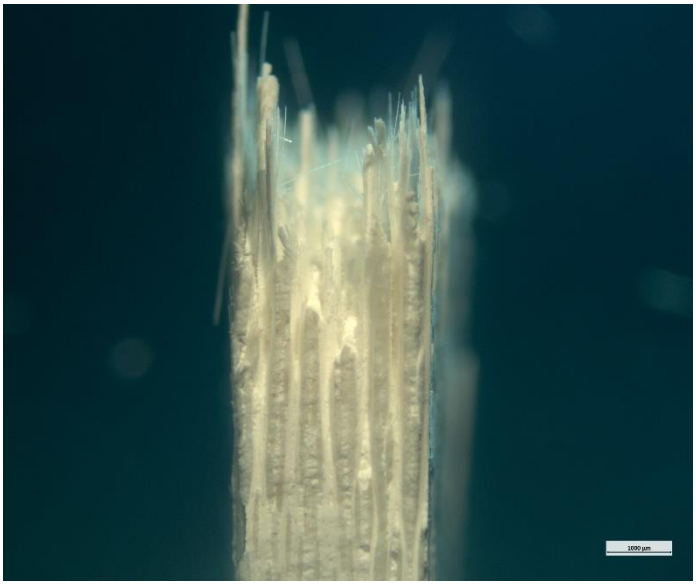

Figure 37. Optical micrograph of the fracture surface of N720/AM specimen tested in tension-tension fatigue at 1200°C in air. σ_{max} = 92 MPa, N_f = 24894.

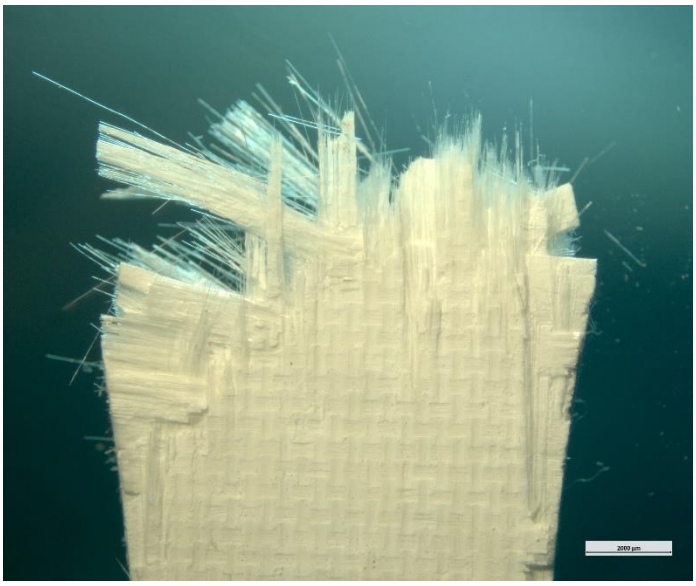

Figure 38. Optical micrograph of the fracture surface of N720/AM specimen tested in tension-tension fatigue at 1200°C in air. σ_{max} = 60 MPa, N_f = 70616.

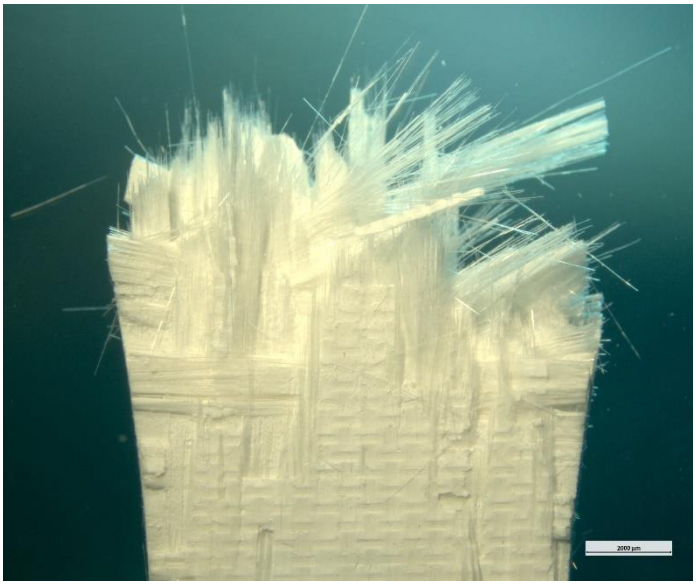

Figure 39. Optical micrograph of the fracture surface of N720/AM specimen tested in tension-tension fatigue at 1200°C in air. σ_{max} = 60 MPa, N_f = 70616.

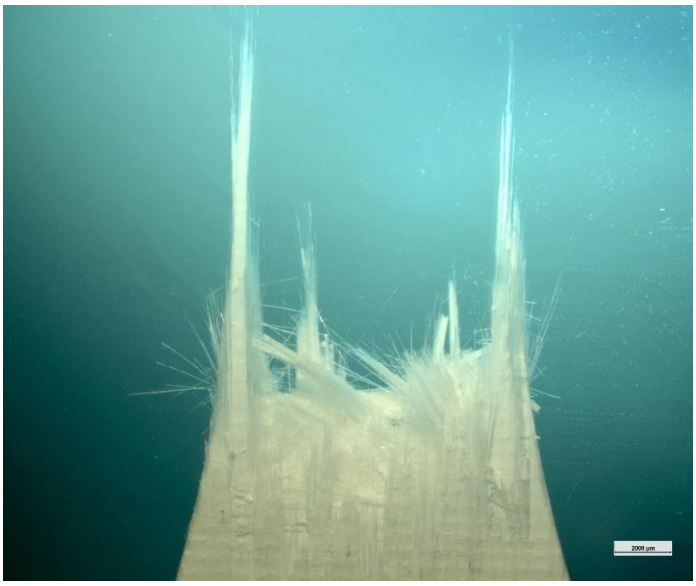

Figure 40. Optical micrograph of the fracture surface of N720/AM specimen tested in tension-tension fatigue at 1200°C in air. σ_{max} = 60 MPa, N_f = 70616.

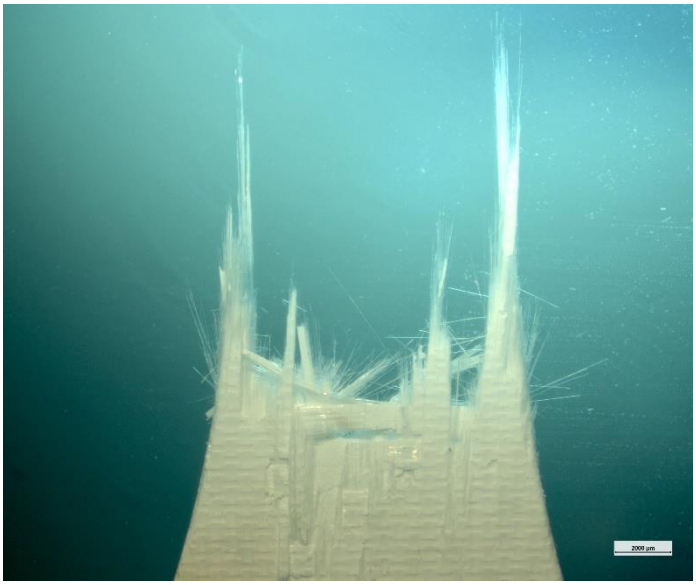

Figure 41. Optical micrograph of the fracture surface of N720/AM specimen tested in tension-tension fatigue at 1200°C in air. σ_{max} = 60 MPa, N_f = 70616.

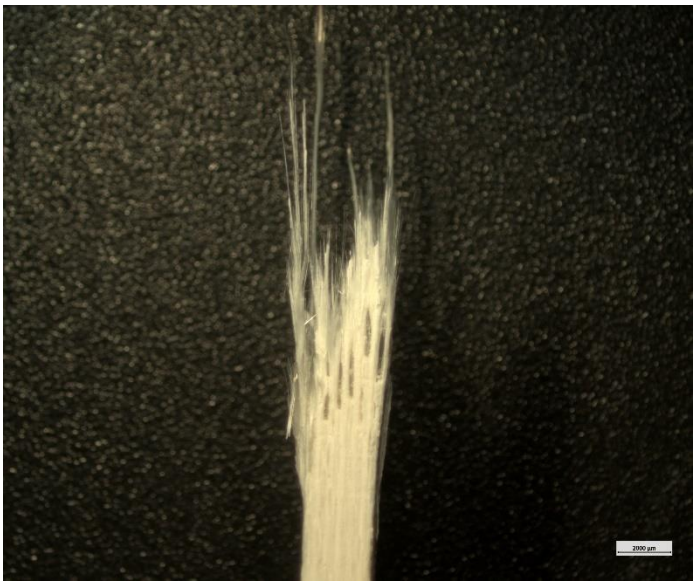

Figure 42. Optical micrograph of the fracture surface of N720/AM specimen tested in tension-tension fatigue at 1200°C in air. σ_{max} = 60 MPa, N_f = 70616.

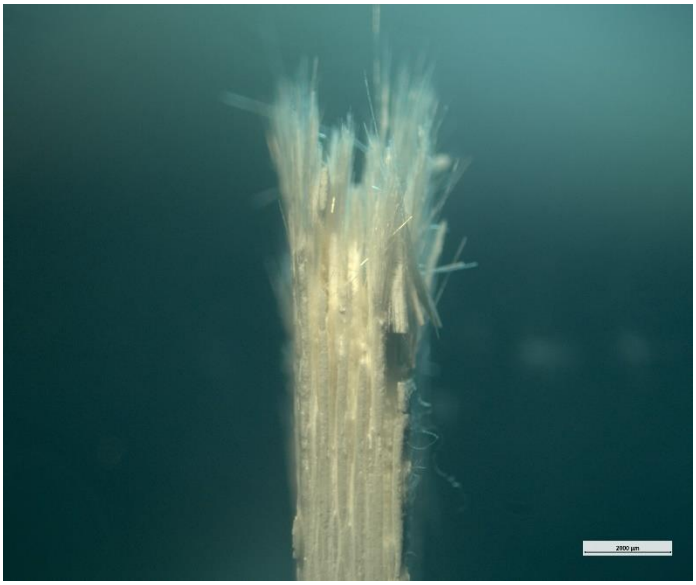

Figure 43. Optical micrograph of the fracture surface of N720/AM specimen tested in tension-tension fatigue at 1200°C in air. σ_{max} = 60 MPa, N_f = 70616.

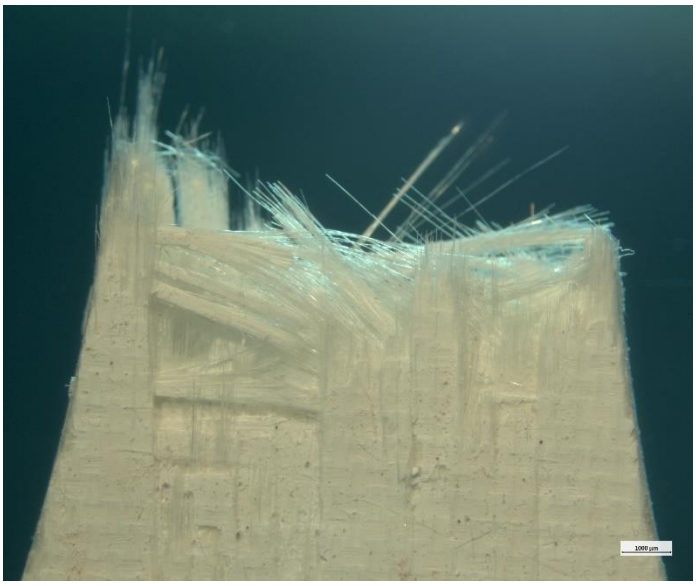

Figure 44. Optical micrograph of the fracture surface of N720/AM specimen tested in tension-tension fatigue at 1200°C in air. σ_{max} = 45 MPa, N_f > 100000.

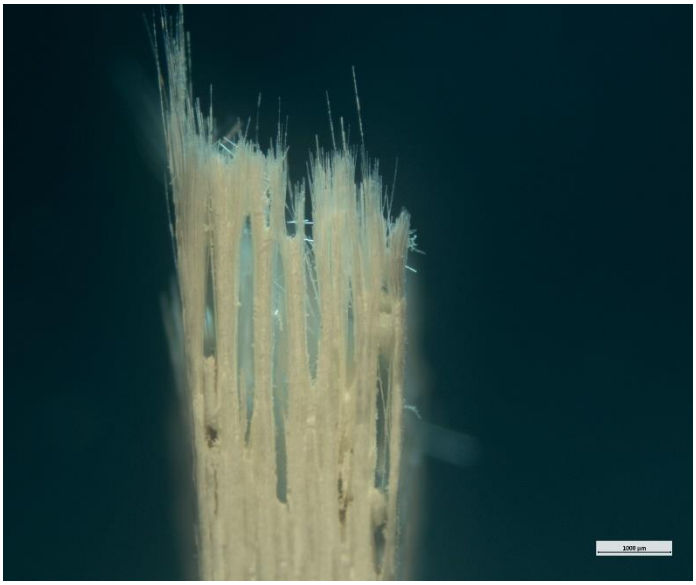

Figure 45. Optical micrograph of the fracture surface of N720/AM specimen tested in tension-tension fatigue at 1200°C in air. σ_{max} = 45 MPa, N_f > 100000.

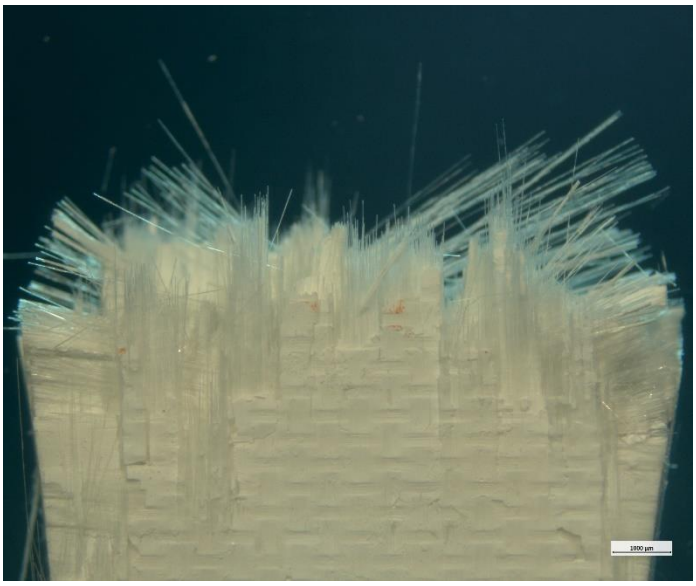

Figure 46. Optical micrograph of the fracture surface of N720/AM specimen tested in tension-tension fatigue at 1200°C in air. σ_{max} = 45 MPa, N_f > 100000.

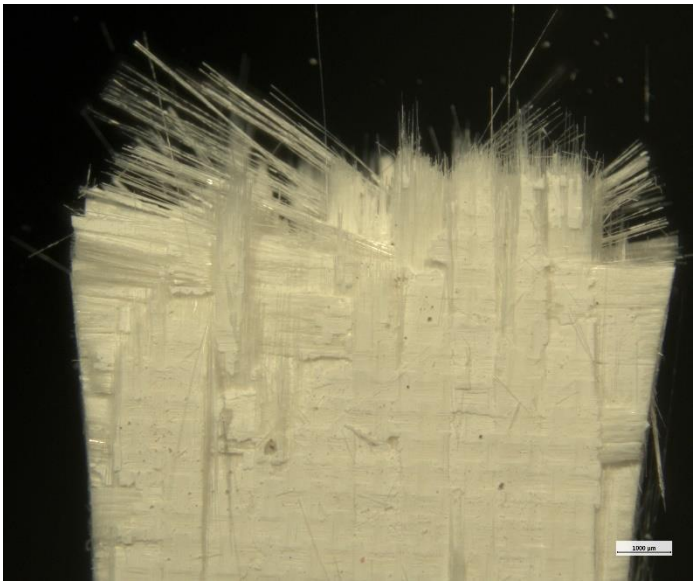

Figure 47. Optical micrograph of the fracture surface of N720/AM specimen tested in tension-tension fatigue at 1200°C in air. σ_{max} = 45 MPa, N_f > 100000.

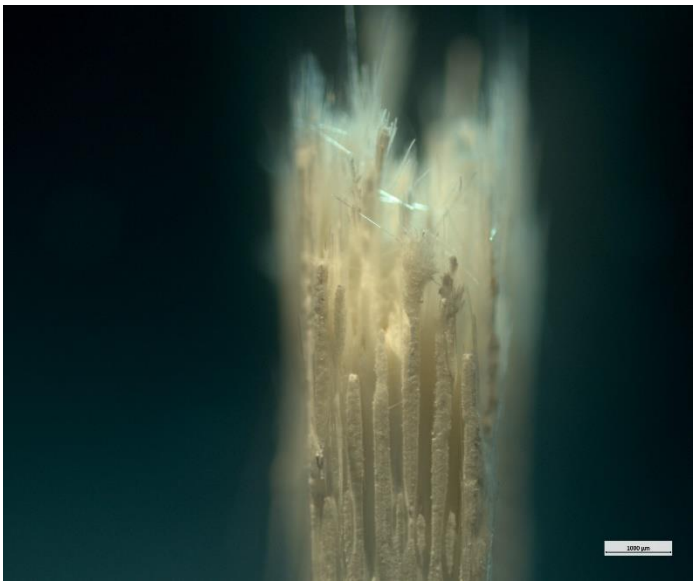

Figure 48. Optical micrograph of the fracture surface of N720/AM specimen tested in tension-tension fatigue at 1200°C in air. σ_{max} = 45 MPa, N_f > 100000.

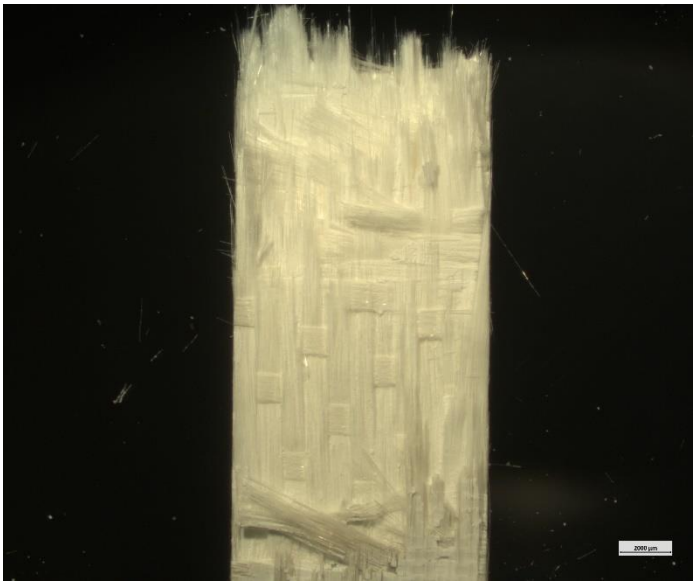

Figure 49. Optical micrograph of the fracture surface of N720/AM specimen tested in tension-tension fatigue at 1200°C in steam. σ_{max} = 136 MPa, N_f = 20212.

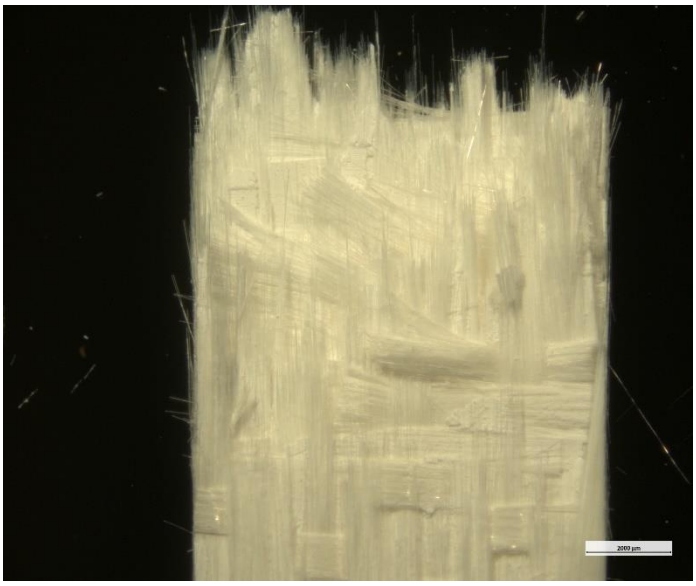

Figure 50. Optical micrograph of the fracture surface of N720/AM specimen tested in tension-tension fatigue at 1200°C in steam. σ_{max} = 136 MPa, N_f = 20212.

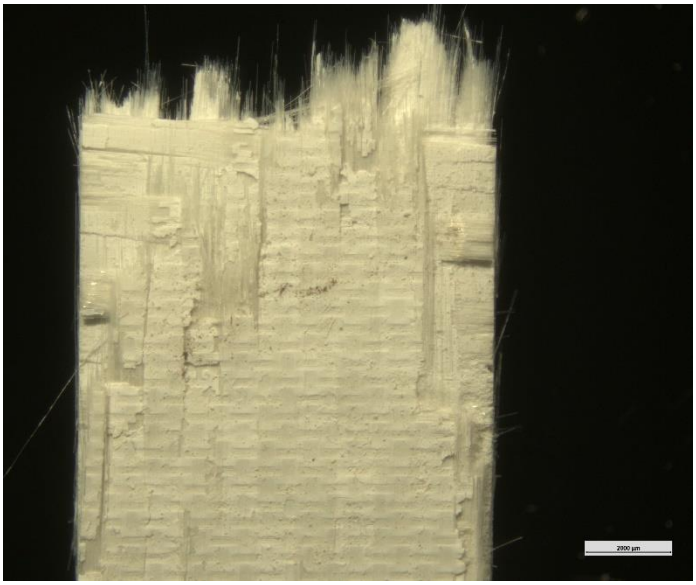

Figure 51. Optical micrograph of the fracture surface of N720/AM specimen tested in tension-tension fatigue at 1200°C in steam. σ_{max} = 136 MPa, N_f = 20212.

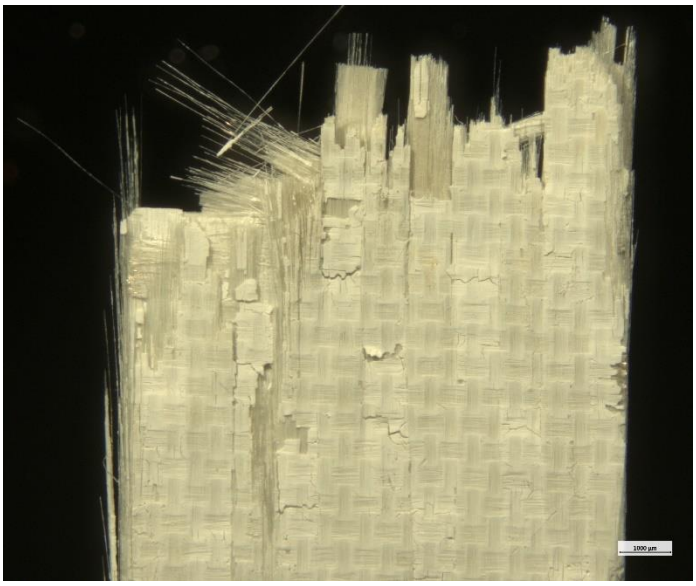

Figure 52. Optical micrograph of the fracture surface of N720/AM specimen tested in tension-tension fatigue at 1200°C in steam. σ_{max} = 136 MPa, N_f = 20212.

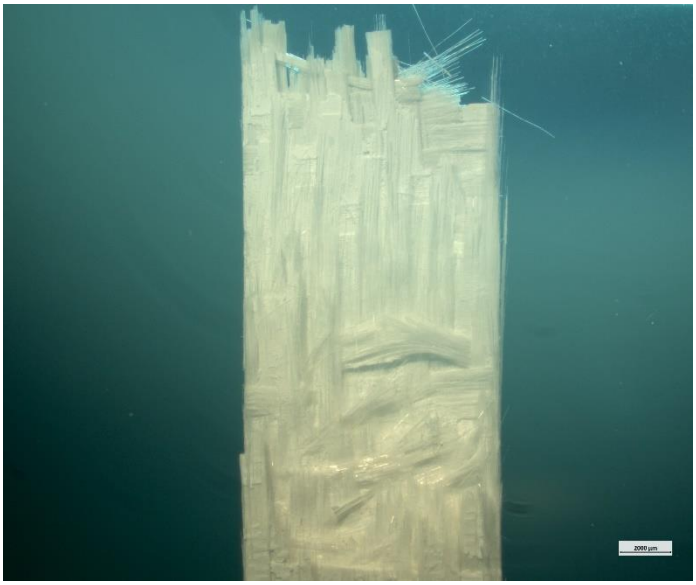

Figure 53. Optical micrograph of the fracture surface of N720/AM specimen tested in tension-tension fatigue at 1200°C in steam. σ_{max} = 136 MPa, N_f = 20212.

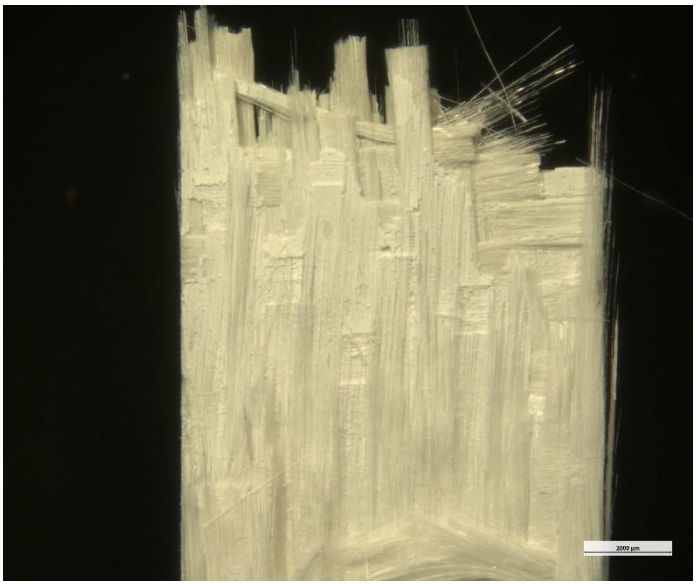

Figure 54. Optical micrograph of the fracture surface of N720/AM specimen tested in tension-tension fatigue at 1200°C in steam. σ_{max} = 136 MPa, N_f = 20212.

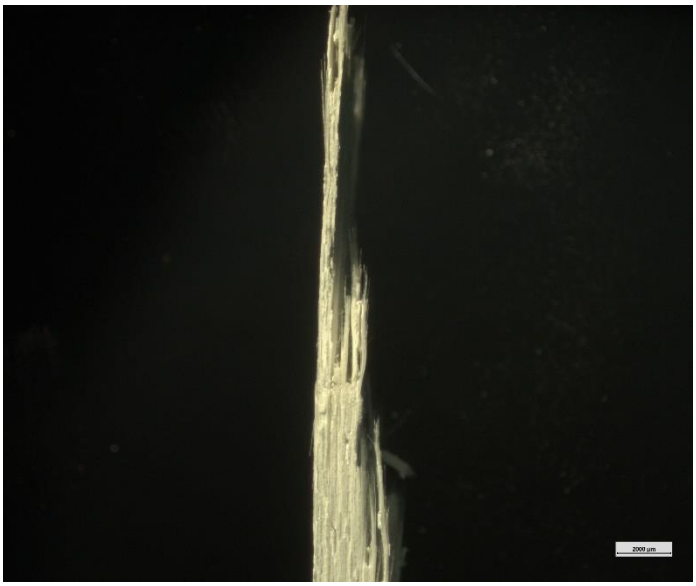

Figure 55. Optical micrograph of the fracture surface of N720/AM specimen tested in tension-tension fatigue at 1200°C in steam. σ_{max} = 136 MPa, N_f = 20212.

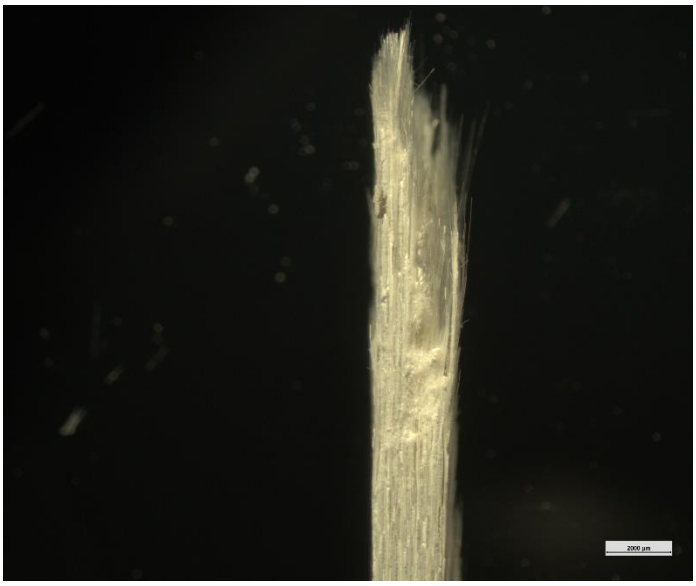

Figure 56. Optical micrograph of the fracture surface of N720/AM specimen tested in tension-tension fatigue at 1200°C in steam. σ_{max} = 136 MPa, N_f = 20212.

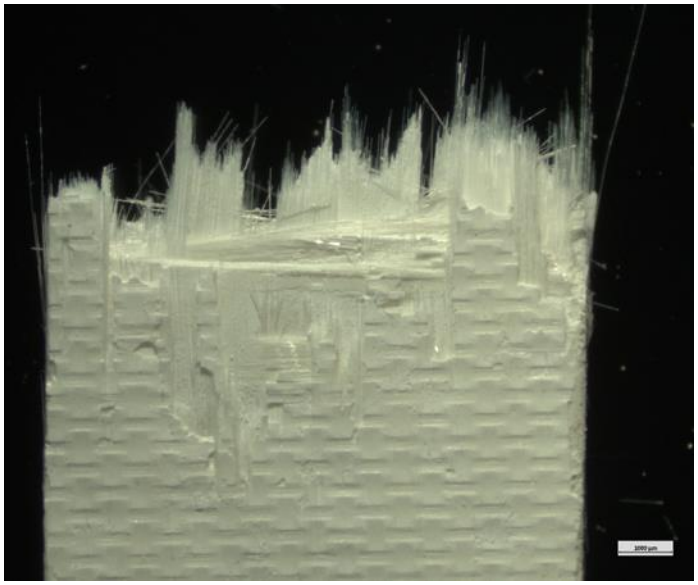

Figure 57. Optical micrograph of the fracture surface of N720/AM specimen tested in tension-tension fatigue at 1200°C in steam. σ_{max} = 120 MPa, N_f > 100000.

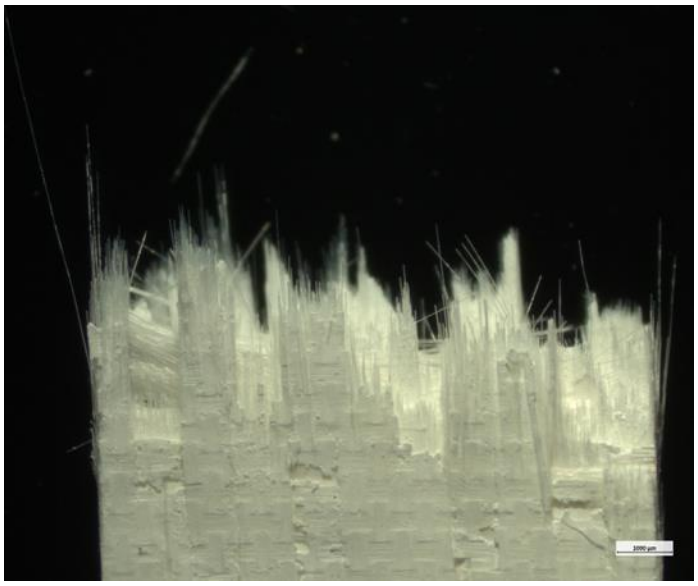

Figure 58. Optical micrograph of the fracture surface of N720/AM specimen tested in tension-tension fatigue at 1200°C in steam. σ_{max} = 120 MPa, N_f > 100000.

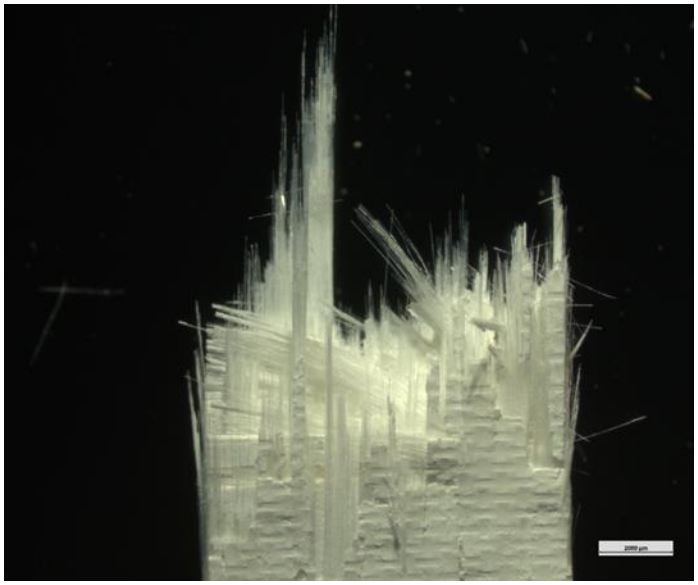

Figure 59. Optical micrograph of the fracture surface of N720/AM specimen tested in tension-tension fatigue at 1200°C in steam. σ_{max} = 120 MPa, N_f > 100000.

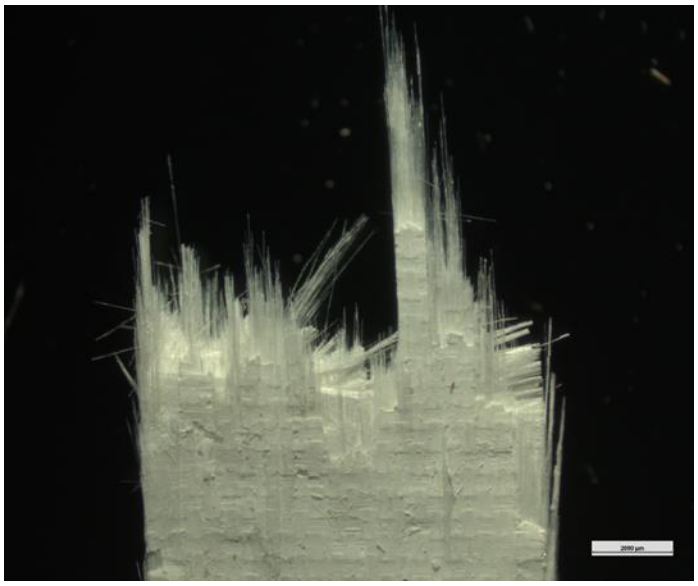

Figure 60. Optical micrograph of the fracture surface of N720/AM specimen tested in tension-tension fatigue at 1200°C in steam. σ_{max} = 120 MPa, N_f > 100000.

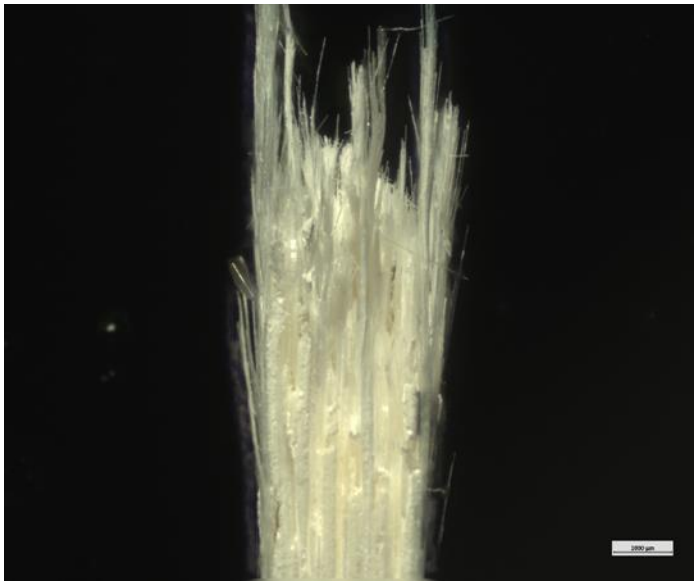

Figure 61. Optical micrograph of the fracture surface of N720/AM specimen tested in tension-tension fatigue at 1200°C in steam. σ_{max} = 120 MPa, N_f > 100000.

Figure 62. Optical micrograph of the fracture surface of N720/AM specimen tested in tension-tension fatigue at 1200°C in steam. σ_{max} = 120 MPa, N_f > 100000.

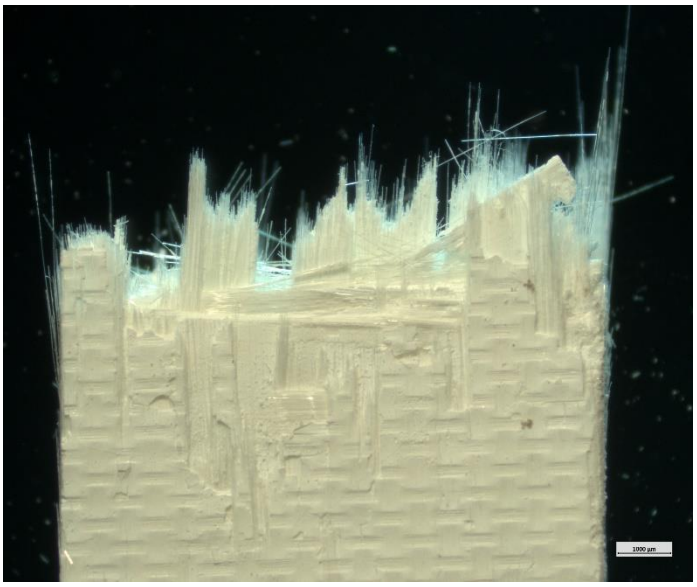

Figure 63. Optical micrograph of the fracture surface of N720/AM specimen tested in tension-tension fatigue at 1200°C in steam. σ_{max} = 92 MPa, N_f > 100000.

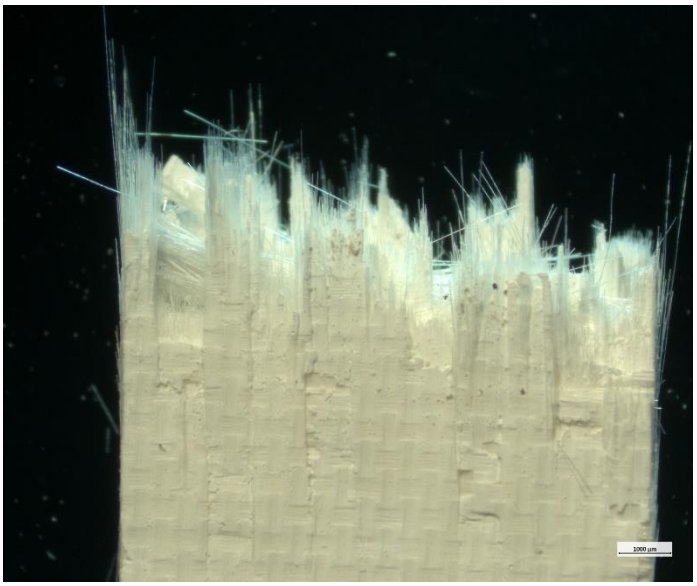

Figure 64. Optical micrograph of the fracture surface of N720/AM specimen tested in tension-tension fatigue at 1200°C in steam. σ_{max} = 92 MPa, N_f > 100000.

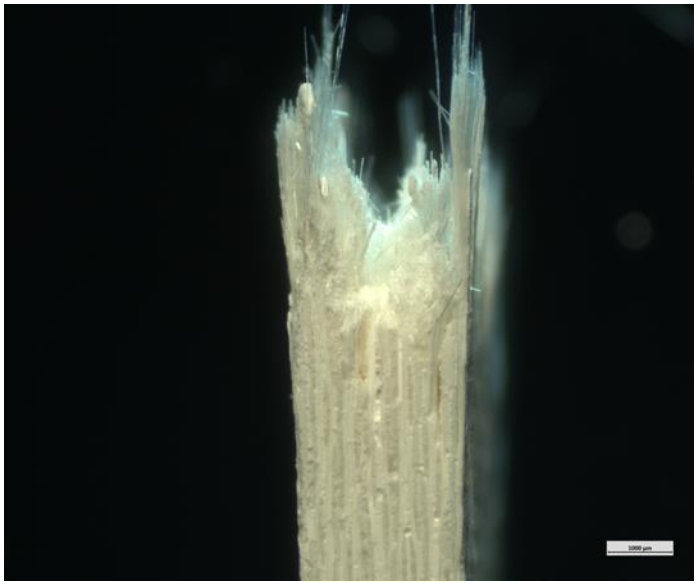

Figure 65. Optical micrograph of the fracture surface of N720/AM specimen tested in tension-tension fatigue at 1200°C in steam. σ_{max} = 92 MPa, N_f > 100000.

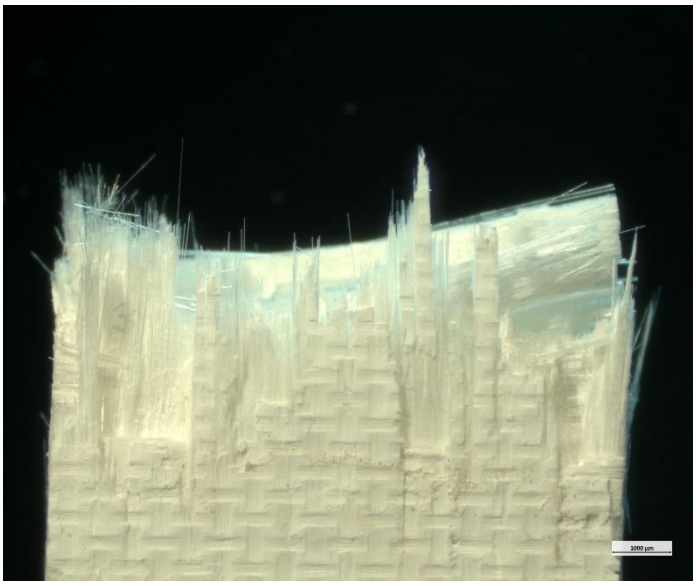

Figure 66. Optical micrograph of the fracture surface of N720/AM specimen tested in tension-tension fatigue at 1200°C in steam. σ_{max} = 92 MPa, N_f > 100000.

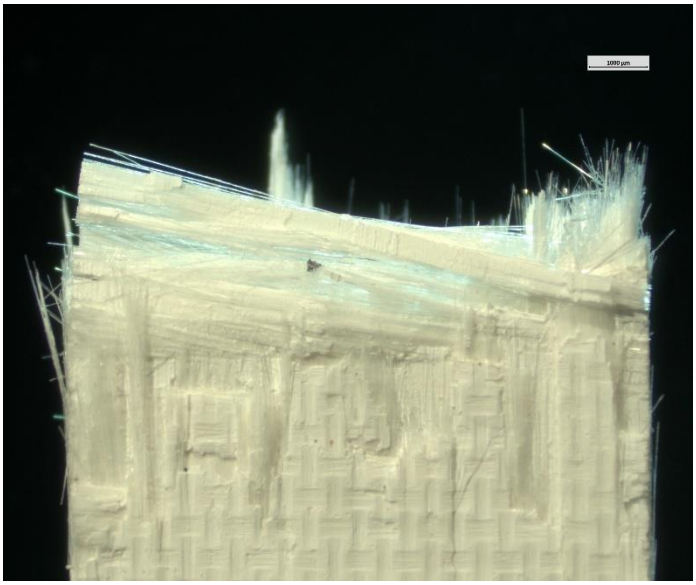

Figure 67. Optical micrograph of the fracture surface of N720/AM specimen tested in tension-tension fatigue at 1200°C in steam. σ_{max} = 92 MPa, N_f > 100000.

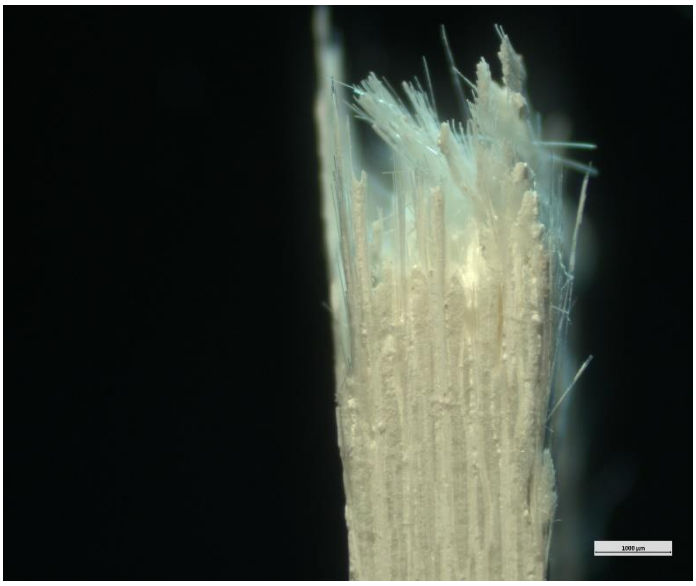

Figure 68. Optical micrograph of the fracture surface of N720/AM specimen tested in tension-tension fatigue at 1200°C in steam. σ_{max} = 92 MPa, N_f > 100000.

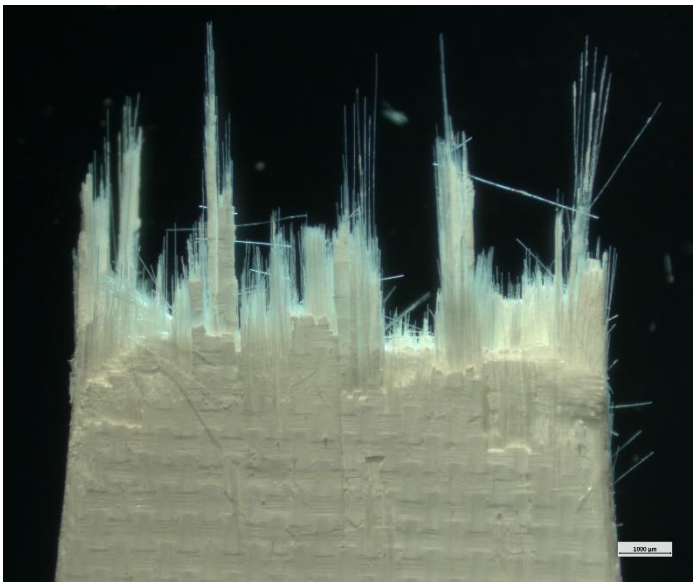

Figure 69. Optical micrograph of the fracture surface of N720/AM specimen tested in tension-tension fatigue at 1200°C in steam. σ_{max} = 60 MPa, N_f > 100000.

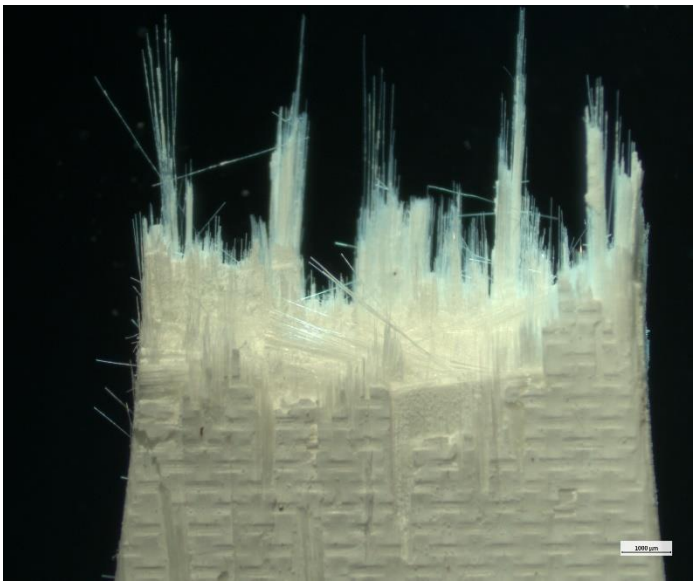

Figure 70. Optical micrograph of the fracture surface of N720/AM specimen tested in tension-tension fatigue at 1200°C in steam. σ_{max} = 60 MPa, N_f > 100000.

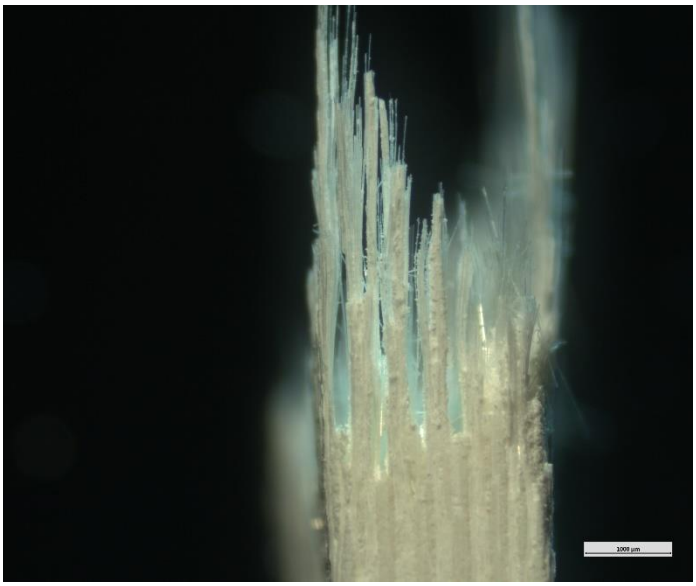

Figure 71. Optical micrograph of the fracture surface of N720/AM specimen tested in tension-tension fatigue at 1200°C in steam. σ_{max} = 60 MPa, N_f > 100000.

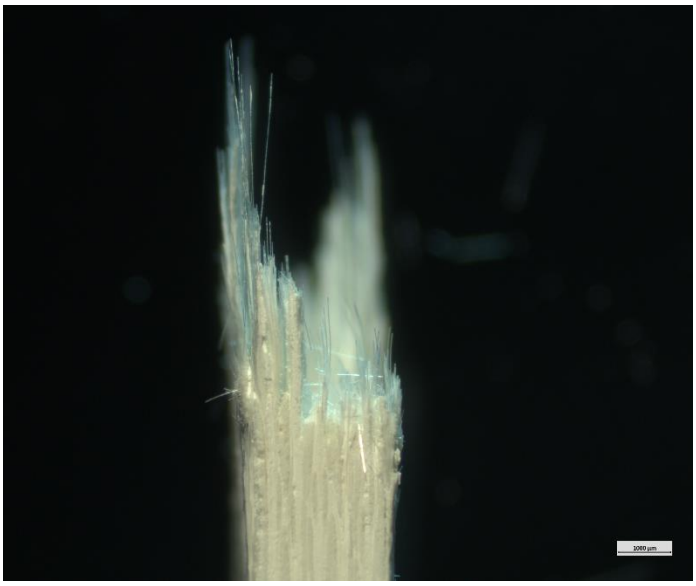

Figure 72. Optical micrograph of the fracture surface of N720/AM specimen tested in tension-tension fatigue at 1200°C in steam. σ_{max} = 60 MPa, N_f > 100000.

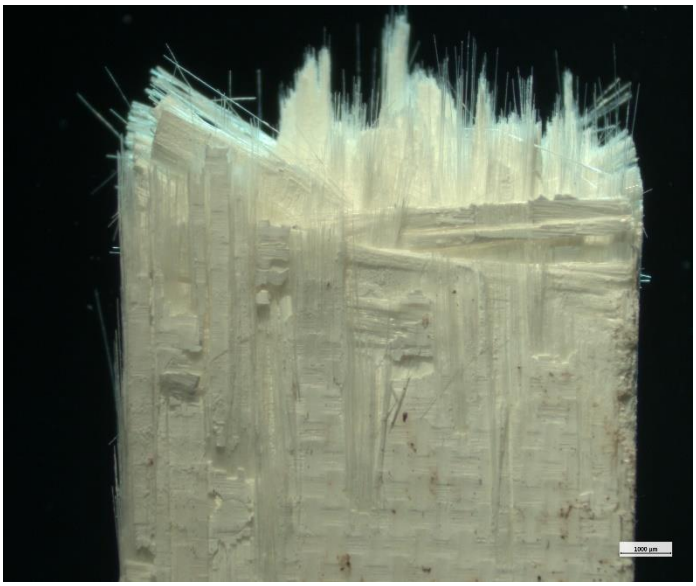

Figure 73. Optical micrograph of the fracture surface of N720/AM specimen tested in tension-tension fatigue at 1200°C in steam. σ_{max} = 60 MPa, N_f > 100000.

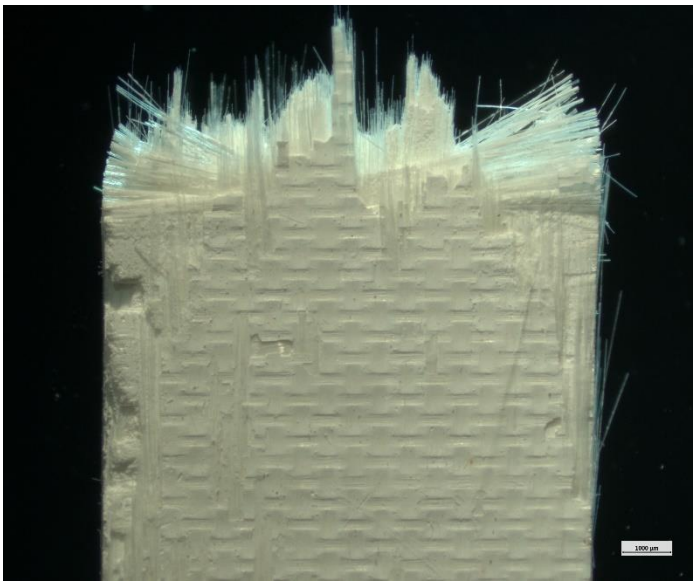

Figure 74. Optical micrograph of the fracture surface of N720/AM specimen tested in tension-tension fatigue at 1200°C in steam. σ_{max} = 60 MPa, N_f > 100000.

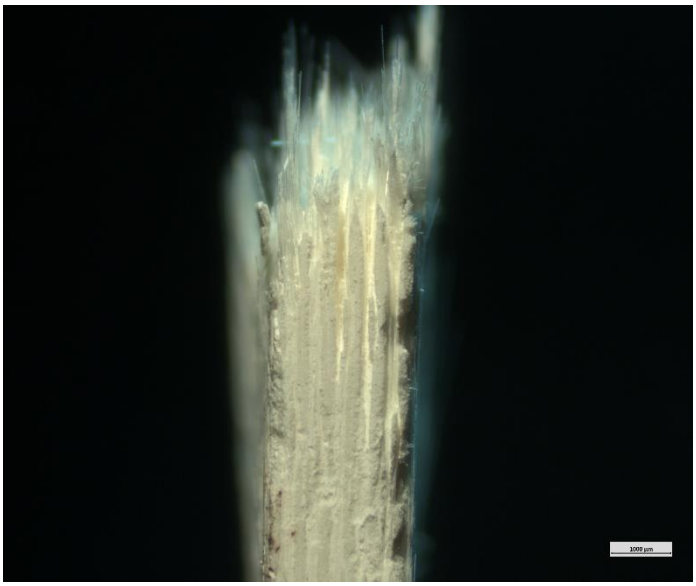

Figure 75. Optical micrograph of the fracture surface of N720/AM specimen tested in tension-tension fatigue at 1200°C in steam. σ_{max} = 60 MPa, N_f > 100000.

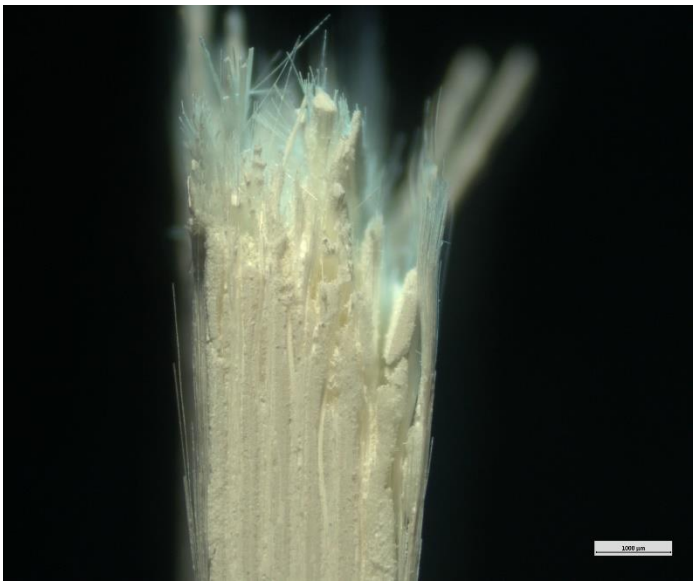

Figure 76. Optical micrograph of the fracture surface of N720/AM specimen tested in tension-tension fatigue at 1200°C in steam. σ_{max} = 60 MPa, N_f > 100000.

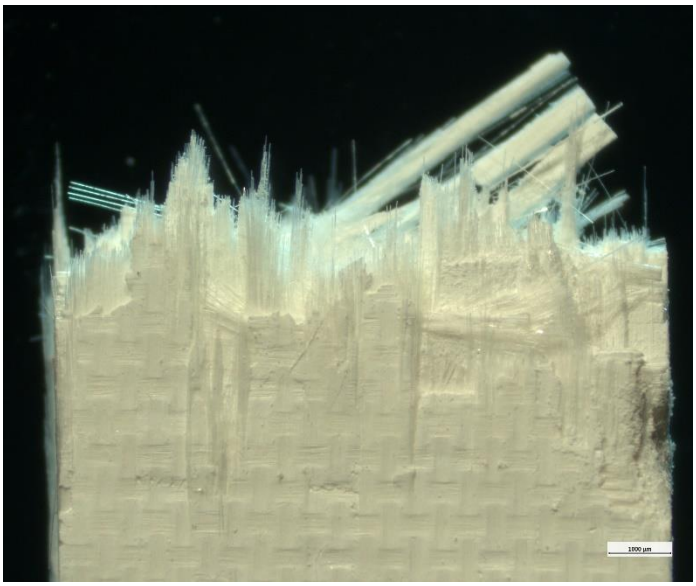

Figure 77. Optical micrograph of the fracture surface of N720/AM specimen tested in tension-tension fatigue at 1200°C in steam. σ_{max} = 60 MPa, N_f > 100000.

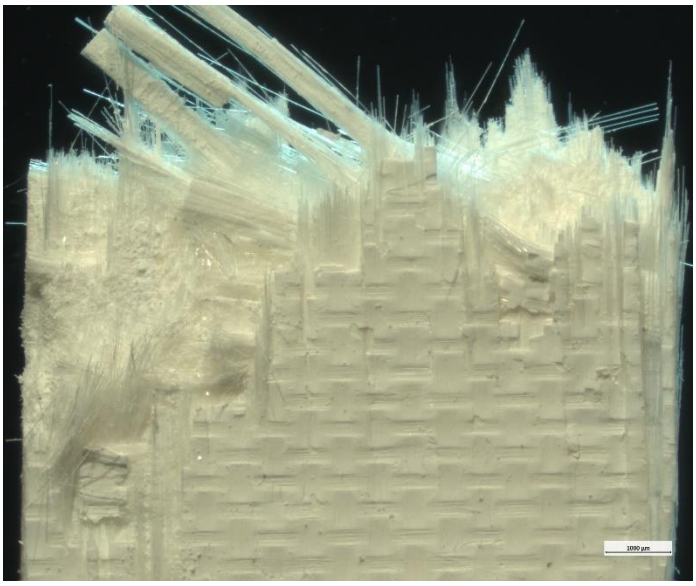

Figure 78. Optical micrograph of the fracture surface of N720/AM specimen tested in tension-tension fatigue at 1200°C in steam. σ_{max} = 60 MPa, N_f > 100000.

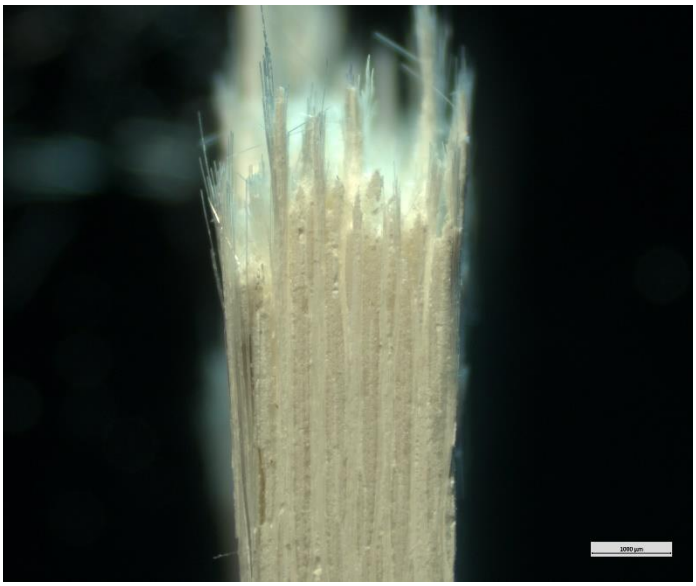

Figure 79. Optical micrograph of the fracture surface of N720/AM specimen tested in tension-tension fatigue at 1200°C in steam. σ_{max} = 60 MPa, N_f > 100000.

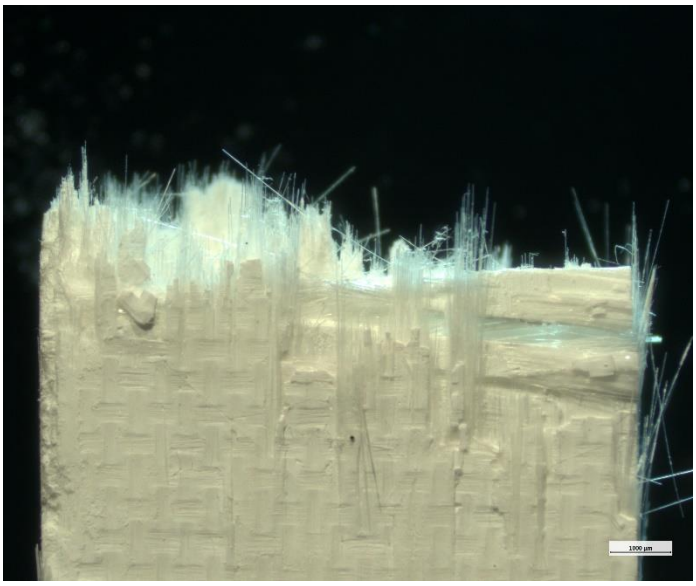

Figure 80. Optical micrograph of the fracture surface of N720/AM specimen tested in tension-tension fatigue at 1200°C in steam. σ_{max} = 60 MPa, N_f > 100000.

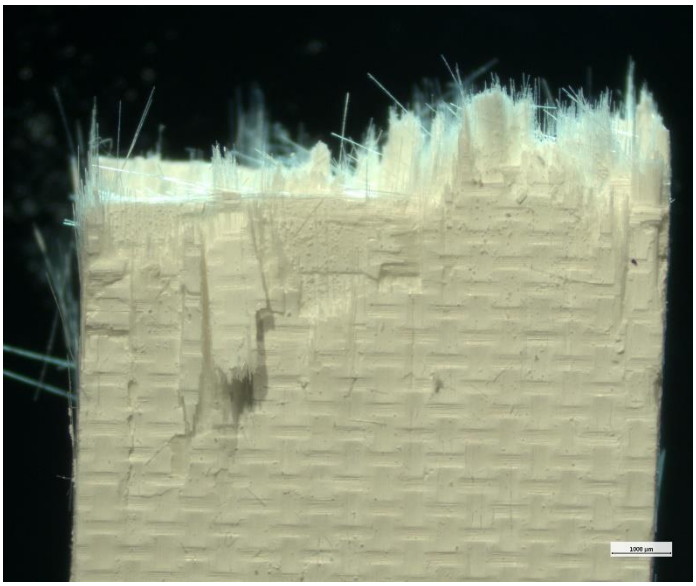

Figure 81. Optical micrograph of the fracture surface of N720/AM specimen tested in tension-tension fatigue at 1200°C in steam. σ_{max} = 60 MPa, N_f > 100000.

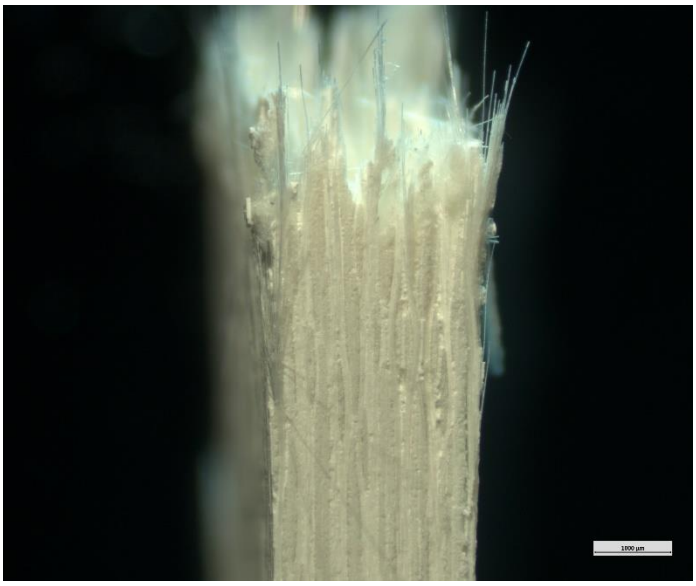

Figure 82. Optical micrograph of the fracture surface of N720/AM specimen tested in tension-tension fatigue at 1200°C in steam. σ_{max} = 60 MPa, N_f > 100000.

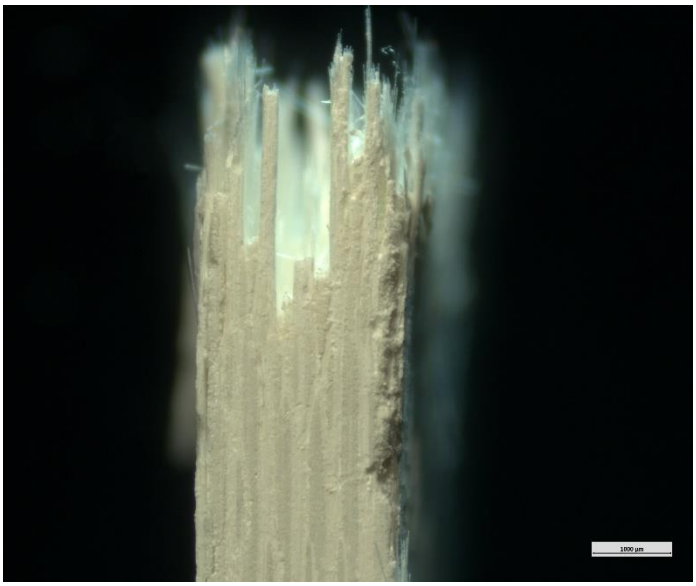

Figure 83. Optical micrograph of the fracture surface of N720/AM specimen tested in tension-tension fatigue at 1200°C in steam. σ_{max} = 60 MPa, N_f > 100000.

Bibliography

[1] I. M. Daniel and O. Ishai, *Engineering Mechanics of Composite Materials*, Second Edi. New York: Oxford University Press, 2006.

[2] A. B. Nair and R. Joseph, "9 - Eco-friendly bio-composites using natural rubber (NR) matrices and natural fiber reinforcements," S. Kohjiya and Y. B. T.-C. Ikeda Manufacture and Applications of Natural Rubber, Eds. Woodhead Publishing, 2014, pp. 249–283.

[3] "Mud Bricks - Global Egyptian Museum," *Global Egyptian Museum*, 2018. [Online]. Available: http://www.globalegyptianmuseum.org/glossary.aspx?id=250. [Accessed: 19-May-2020].

[4] A. R. Bunsell and J. Renard, *Fundamentals of Fibre Reinforced Composite Materials*. CRC Press, 2005.

[5] "Ceramic Matrix Composites Market in Aircraft Engines," 2018.

[6] C. E. (SAE) Howard, "Ceramic matrix composites in aircraft engines projected to double over five years," *SAE Interanational*, 2018. [Online]. Available: https://www.sae.org/news/2018/07/ceramic-matrix-composites-in-aircraft-engines-projected-to-double-over-five-years-stratview-research-predicts.

[7] F. C. Campbell, "Introduction to Composite Materials," *ASM Int.*, 2010, doi: 10.1201/9781315367965-6.

[8] T. Siddiqui, "Composites," New York: McGraw-Hill Education, 2015.

[9] W. C. Young, R. G. Budynas, A. M. Sadegh, and P. Notice, "Composite Materials," 8th ed. /., New York: McGraw-Hill Education, 2012.

[10] D. Eliche-Quesada, L. Pérez-Villarejo, and P. Sánchez-Soto, "Introduction to Ceramic Materials: Synthesis, Characterization, Applications, and Recycling," 2019.

[11] F. Rebillat, *Advances in self-healing ceramic matrix composites*. Woodhead Publishing Limited, 2014.

[12] R. Jones, C. Henager, C. Lewinsohn, and C. Windisch, "Ceramic Matrix Composites," 2001, pp. 391–418.

[13] H. Ohnabe, S. Masaki, M. Onozuka, K. Miyahara, and T. Sasa, "Potential application of ceramic matrix composites to aero-engine components," *Compos. Part A Appl. Sci. Manuf.*, vol. 30, no. 4, pp. 489–496, 1999, doi: 10.1016/S1359-835X(98)00139-0.

[14] I. M. Low, *Advances in ceramic matrix composites: Introduction*, no. 1. Elsevier Ltd, 2018.

[15] C. P. Yang, L. Zhang, B. Wang, T. Huang, and G. Q. Jiao, "Tensile behavior of 2D-C/SiC composites at elevated temperatures: Experiment and modeling," *J. Eur. Ceram. Soc.*, vol. 37, no. 4, pp. 1281–1290, 2017, doi: 10.1016/j.jeurceramsoc.2016.11.011.

[16] "Ceramic Matrix Composites (Introduction)," no. Cmc.

[17] M. B. Ruggles-Wrenn, *Mechanical behavior of oxide-oxide fiber-reinforced CMCs at elevated temperature: Environmental effects*, vol. 5. 2017.

[18] D. M. Wilson and L. R. Visser, “High performance oxide fibers for metal and ceramic composites,” *Compos. - Part A Appl. Sci. Manuf.*, vol. 32, no. 8, pp. 1143–1153, 2001, doi: 10.1016/S1359-835X(00)00176-7.
[19] H. E. Boyer, “Fatigue Testing,” *Www.Astminternational.Org*, vol. 1, 1986.
[20] C. Genelin, “EFFECTS OF ENVIRONMENT ON CREEP BEHAVIOR OF NEXTEL 720/ALUMINA-MULLITE CERAMIC COMPOSITE AT 1200°C,” 2008.
[21] M. Ozer and M. B. Ruggles-Wrenn, “Effects of Environment on Creep Behavior of NextelTM 720/Alumina-Mullite Ceramic Composite with ±45° Fiber Orientation at 1200°C,” 2010, pp. 245–260.
[22] T. Kutsal, “Effect of Steam Environment on Creep Behavior of Nextel720/Alumina-Mullite Ceramic Matrix Composite At Elevated Temperature,” 2009.
[23] C. Kaya, E. G. Butler, A. Selcuk, A. R. Boccaccini, and M. H. Lewis, “Mullite (NextelTM 720) fibre-reinforced mullite matrix composites exhibiting favourable thermomechanical properties,” *J. Eur. Ceram. Soc.*, 2002, doi: 10.1016/S0955-2219(01)00531-3.
[24] R. A. Jurf and S. C. Butner, “Advances in oxide-oxide CMC,” in *Journal of Engineering for Gas Turbines and Power*, 2000, doi: 10.1115/1.483195.
[25] M. B. Ruggles-Wrenn and C. L. Genelin, “Creep of Nextel™720/alumina-mullite ceramic composite at 1200 °C in air, argon, and steam,” *Compos. Sci. Technol.*, vol. 69, no. 5, pp. 663–669, 2009, doi: 10.1016/j.compscitech.2009.01.002.
[26] M. B. Ruggles-Wrenn and M. Ozer, “Creep behavior of Nextel™720/alumina-mullite ceramic composite with ±45° fiber orientation at 1200°C,” *Mater. Sci. Eng. A*, vol. 527, no. 20, pp. 5326–5334, 2010, doi: 10.1016/j.msea.2010.05.030.

REPORT DOCUMENTATION PAGE

Form Approved
OMB No. 074-0188

PLEASE DO NOT RETURN YOUR FORM TO THE ABOVE ADDRESS.

1. REPORT DATE *(DD-MM-YYYY)*	**2. REPORT TYPE**	**3. DATES COVERED** *(From – To)*
09-07-2020	Master's Thesis	October 2018 – July 2020

TITLE AND SUBTITLE

Tension-Tension Fatigue Behavior of Nextel 720/Alumina-Mullite Ceramic Composite at 1200°C in Air and Steam

5a. CONTRACT NUMBER

5b. GRANT NUMBER

5c. PROGRAM ELEMENT NUMBER

6. AUTHOR(S)

Witzgall, Sarah A., 1st Lt, USAF

5d. PROJECT NUMBER

5e. TASK NUMBER

5f. WORK UNIT NUMBER

7. PERFORMING ORGANIZATION NAMES(S) AND ADDRESS(S)

Air Force Institute of Technology
Graduate School of Engineering and Management (AFIT/ENY)
2950 Hobson Way, Building 640
WPAFB OH 45433-8865

8. PERFORMING ORGANIZATION REPORT NUMBER

AFIT-ENY-MS-20-J-087

9. SPONSORING/MONITORING AGENCY NAME(S) AND ADDRESS(ES)

Intentionally left blank

10. SPONSOR/MONITOR'S ACRONYM(S)

11. SPONSOR/MONITOR'S REPORT NUMBER(S)

12. DISTRIBUTION/AVAILABILITY STATEMENT

DISTRUBTION STATEMENT A. APPROVED FOR PUBLIC RELEASE; DISTRIBUTION UNLIMITED.

13. SUPPLEMENTARY NOTES

14. ABSTRACT

Uniaxial tension-tension fatigue performance of an oxide-oxide continuous fiber ceramic composite was studied at 1200°C in laboratory air and in steam. The composite is reinforced with laminated, 0/90 mullite/alumina (NEXTEL™720) fibers woven in an eight-harness satin weave and has a porous alumina/mullite matrix. There is no interphase between the fiber and matrix. The composite relies on the porous matrix for crack deflection and flaw tolerance. Tension-tension fatigue was examined for maximum stresses of 45 – 136 MPa in air and in steam. To assess the effects of the steam environment on fatigue performance, experimental results obtained in air are compared to those obtained in steam. The retained properties of all specimens that achieved fatigue run-out were characterized. Composite microstructure, as well as damage and failure mechanisms, were examined.

15. SUBJECT TERMS

Ceramic Matrix Composite, Tension-Tension Fatigue, Oxide-Oxide CMC, Porous Alumina/Mullite Matrix, Nextel 720 Fibers

16. SECURITY CLASSIFICATION OF:			**17. LIMITATION OF ABSTRACT**	**18. NUMBER OF PAGES**	**19a. NAME OF RESPONSIBLE PERSON**
a. REPORT	**b. ABSTRACT**	**c. THIS PAGE**			Dr. Marina B. Ruggles-Wrenn, AFIT/ENY
U	**U**	**U**	**UU**	94	**19b. TELEPHONE NUMBER** *(Include area code)* (937) 255-6565, ext 4641 (marina.ruggles-wrenn@afit.edu)

Standard Form 298 (Rev. 8-98)
Prescribed by ANSI Std. Z39-18